Persistence of Drug-Resistant Leukemic Stem Cells and Impaired NK Cell Immunity in CML Patients Depend on *MIR300* Antiproliferative and PP2A-Activating Functions

Giovannino Silvestri[1,2], Rossana Trotta[2,3], Lorenzo Stramucci[1,2], Justin J. Ellis[4,5], Jason G. Harb[4,5], Paolo Neviani[4,5], Shuzhen Wang[1], Ann-Kathrin Eisfeld[4,5], Christopher J. Walker[4,5], Bin Zhang[6], Klara Srutova[7], Carlo Gambacorti-Passerini[8], Gabriel Pineda[9], Catriona H.M. Jamieson[10], Fabio Stagno[11], Paolo Vigneri[11], Georgios Nteliopoulos[12], Philippa C. May[12], Alistair G. Reid[12], Ramiro Garzon[4,5], Denis-Claude Roy[13], Moutuaata M. Moutuou[13], Martin Guimond[13], Peter Hokland[14], Michael W. Deininger[15], Garrett Fitzgerald[16], Christopher Harman[16], Francesco Dazzi[17], Dragana Milojkovic[12], Jane F. Apperley[12], Guido Marcucci[6], Jianfei Qi[2], Katerina Machova Polakova[7], Ying Zou[2], Xiaoxuan Fan[2], Maria R. Baer[1,2], Bruno Calabretta[18], and Danilo Perrotti[1,2,12,19]

ABSTRACT

Persistence of drug-resistant quiescent leukemic stem cells (LSC) and impaired natural killer (NK) cell immune response account for relapse of chronic myelogenous leukemia (CML). Inactivation of protein phosphatase 2A (PP2A) is essential for CML-quiescent LSC survival and NK cell antitumor activity. Here we show that *MIR300* has antiproliferative and PP2A-activating functions that are dose dependently differentially induced by CCND2/CDK6 and SET inhibition, respectively. *MIR300* is upregulated in CML LSCs and NK cells by bone marrow microenvironment (BMM) signals to induce quiescence and impair immune response, respectively. Conversely, BCR-ABL1 downregulates *MIR300* in CML progenitors to prevent growth arrest and PP2A-mediated apoptosis. Quiescent LSCs escape apoptosis by upregulating *TUG1* long noncoding RNA that uncouples and limits *MIR300* function to cytostasis. Genetic and pharmacologic *MIR300* modulation and/or PP2A-activating drug treatment restore NK cell activity, inhibit BMM-induced growth arrest, and selectively trigger LSC apoptosis *in vitro* and in patient-derived xenografts; hence, the importance of *MIR300* and PP2A activity for CML development and therapy.

SIGNIFICANCE: Tumor-naïve microenvironment–induced *MIR300* is the only tumor suppressor miRNA that induces CML LSC quiescence while inhibiting NK cell antitumor immune response, and CML LSC/progenitor cell apoptosis through its anti-proliferative and PP2A-activating functions, respectively. Thus, the importance of *MIR300* and PP2A-activating drugs for formation/survival and eradication of drug-resistant CML LSCs, respectively.

See related commentary by Broxmeyer, p. 13.

[1]Department of Medicine, University of Maryland School of Medicine, Baltimore, Maryland. [2]Marlene and Stewart Greenebaum Comprehensive Cancer Center, University of Maryland School of Medicine, Baltimore, Maryland. [3]Department of Microbiology and Immunology, University of Maryland School of Medicine, Baltimore, Maryland. [4]Department of Molecular Virology Immunology and Medical Genetics, The Ohio State University Comprehensive Cancer Center, Columbus, Ohio. [5]Department of Internal Medicine, The Ohio State University Comprehensive Cancer Center, Columbus, Ohio. [6]Division of Hematopoietic Stem Cell and Leukemia Research, City of Hope National Medical Center, Duarte, California. [7]Institute of Hematology and Blood Transfusion, University of Prague, Prague, Czech Republic. [8]Hematology and Clinical Research Unit, San Gerardo Hospital, Monza, Italy. [9]Department of Health Sciences, School of Health and Human Services, National University, San Diego, California. [10]Department of Medicine and Moores Cancer Center, University of California, San Diego, La Jolla, California. [11]Division of Hematology and Unit of Medical Oncology, A.O.U. "Policlinico-Vittorio Emanuele", University of Catania, Catania, Italy. [12]Department of Haematology, Hammersmith Hospital, Imperial College London, London, United Kingdom. [13]Department of Hematology and Cellular Therapy Laboratory, Hôpital Maisonneuve-Rosemont, University of Montreal, Montreal, Quebec, Canada. [14]Department of Hematology, Aarhus University Hospital, Aarhus, Denmark. [15]Division of Hematology and Hematologic Malignancies and Huntsman Cancer Institute, University of Utah, Salt Lake City, Utah. [16]Center for Advanced Fetal Care University, University of Maryland School of Medicine, Baltimore, Maryland. [17]Division of Cancer Studies, Rayne Institute, King's College London, London, United Kingdom. [18]Sidney Kimmel Cancer Center, Thomas Jefferson University, Philadelphia, Pennsylvania. [19]Department of Biochemistry and Molecular Biology, University of Maryland School of Medicine, Baltimore, Maryland.

Note: Supplementary data for this article are available at Blood Cancer Discovery Online (https://bloodcancerdiscov.aacrjournals.org).

G. Silvestri and R. Trotta contributed equally to this article.

Corresponding Author: Danilo Perrotti, University of Maryland, 655 W. Baltimore St., Room 8-045, Baltimore, MD 21201. Phone: 267-968-4562; E-mail: dperrotti@som.umaryland.edu

Blood Cancer Discov 2020;1:48–67

doi: 10.1158/2643-3249.BCD-19-0039

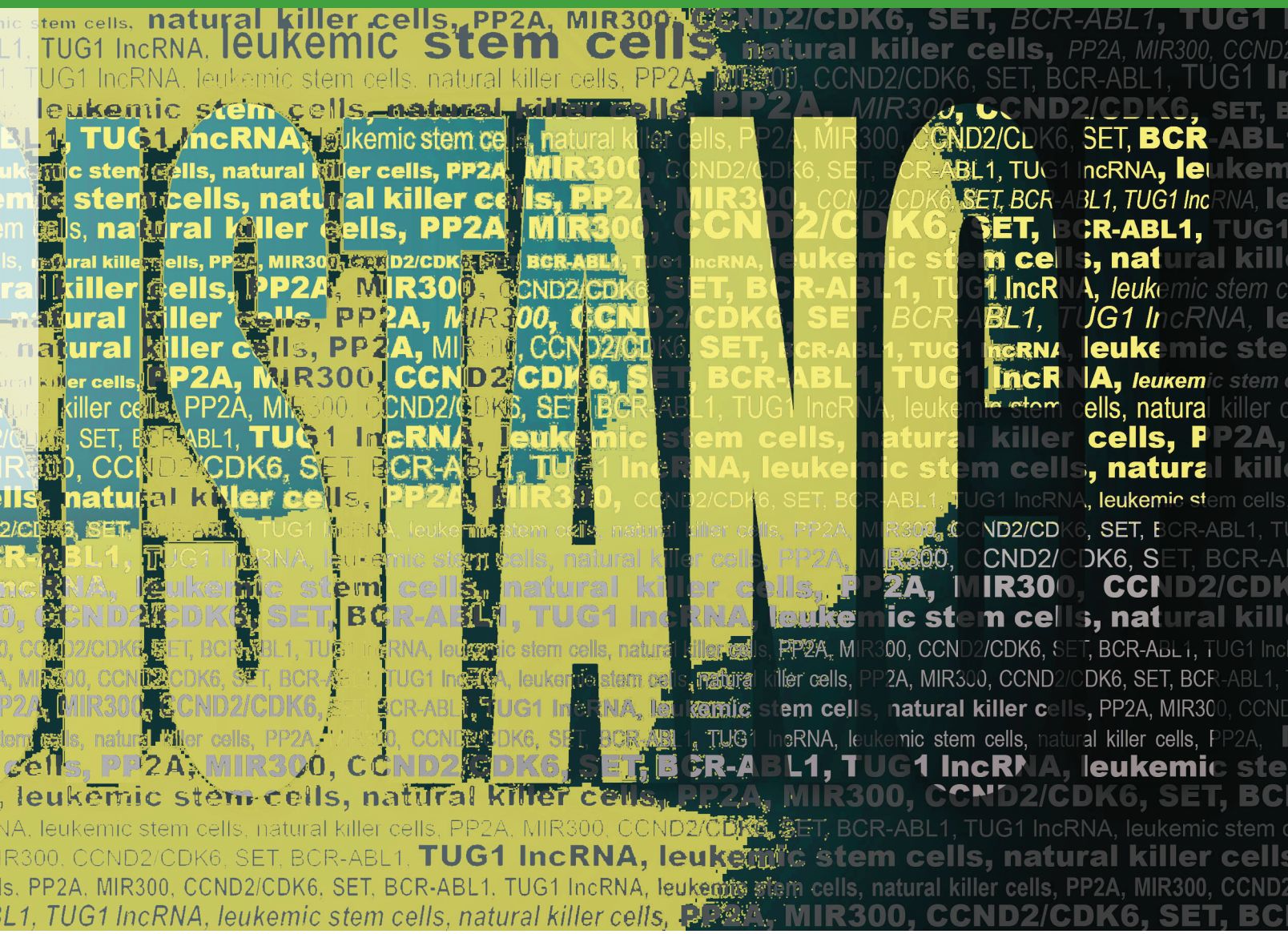

INTRODUCTION

Chronic myeloid leukemia (CML) is a biphasic hematopoietic stem cell (HSC) myeloproliferative disorder driven by BCR-ABL1 oncogenic kinase activity (1). Despite being clinically manageable, CML is not a curable cancer and resistance to ABL tyrosine kinase inhibitors (TKI) remains a major therapeutic challenge (2). In fact, persistence of CML-initiating quiescent leukemic stem cells (qLSC) likely depends on their innate and acquired TKI resistance (3) and on impaired natural killer (NK) cell cytotoxicity against leukemic stem cells (LSC) (4), and accounts for disease relapse and dismal outcome (1, 5). Clinical trials, aimed at targeting intrinsic mechanisms of TKI resistance, failed to eradicate the TKI-resistant qLSC reservoir, likely because of bone marrow (BM) microenvironment (BMM) protective and inhibitory effects on LSCs and NK cells, respectively (5, 6).

Protein phosphatase 2A (PP2A) serine-threonine phosphatase is a druggable multimeric tumor suppressor inactivated in nearly all types of cancer, mostly by increased endogenous inhibitor (e.g., SET, CIP2A) or impaired subunit expression/function (7). PP2A loss-of-function is essential for cancer stem cell maintenance, tumor growth/progression, and activation of NK cell proliferation and antitumor cytotoxic activity (7). BCR-ABL1–independent and -dependent signals inhibit PP2A activity in CML [chronic (CP) and blastic (BC) phase] TKI-resistant qLSCs and TKI-sensitive and -resistant proliferating blasts, respectively, through activation of the SET-dependent PP2A inhibitory pathway (PIP; refs. 8, 9). Preclinical studies aimed at restoring physiologic PP2A activity with SET-sequestering PP2A-activating drugs (PADs; e.g., FDA-approved FTY720, OSU-2S, and OP449) have shown unprecedented antileukemia effects in TKI-sensitive and -resistant CP and BC phase CML qLSCs and progenitors with neither adverse effects on normal hematopoiesis

nor organ toxicity (8–10). In contrast, PP2A inhibiting drugs (PIDs; e.g., LB100), alone and in combination with TKIs, arrest proliferation of TKI-resistant CML progenitors, but do not exert effects on qLSC survival, and enhance leukemogenesis when used alone (11, 12).

The mechanisms underlying CML LSC quiescence, survival and self-renewal, and reduced NK-cell number and cytotoxicity likely result from integration of CML cell–autonomous and BMM-generated signals (1, 6). The latter are triggered by BM niche–specific metabolic conditions (e.g., oxygen tension), cell-to-cell direct, and soluble and/or exosome-encapsulated factor [e.g., microRNA (miRNA)]-mediated interactions between leukemic, mesenchymal stromal (MSC), endothelial, and immune cells (13–15).

Several miRNAs have been associated with PP2A inactivation (16) and LSC expansion and maintenance (17, 18); however, a clear causal link between their altered expression, persistence of drug-resistant LSCs, and PP2A loss-of-function is still missing.

Among the miRNAs predicted *in silico* to reactivate PP2A by targeting PIP factors (e.g., JAK2, hnRNPA1, and SET), we focused on hsa-*miR-300* (*MIR300*), an intergenic miRNA that is inhibited in several stem cell–driven tumors and belongs to the 14q32.31 *DLK1-DIO3* genomic–imprinted tumor suppressor miRNA cluster B (19). Here we report that *MIR300* is a BMM-induced cell context–independent tumor suppressor with antiproliferative and PP2A-activating functions that are not only essential for induction and maintenance of LSC quiescence and impaired NK cell anticancer immunity, but they can also be exploited to selectively and efficiently induce PP2A-mediated cell death of CD34$^+$ CML-quiescent LSCs and proliferating progenitors while sparing normal hematopoiesis.

RESULTS

MIR300 Loss in Leukemic Progenitors and Differential Induction of Its Cell Context–Independent Tumor Suppressor Activities in TKI-Resistant Quiescent CML (CP and BC) LSCs

MIR300 levels were progressively and markedly reduced by BCR-ABL1 activity (imatinib treatment) in bulk and dividing BM CD34$^+$ CML (CP and BC) progenitors compared with normal CD34$^+$ BM (NBM) and umbilical cord blood (UCB) cells, and higher in HSC-enriched CD34$^+$CD38$^-$ than committed CD34$^+$CD38$^+$ CML (CP and BC) BM cells (Fig. 1A). Accordingly, *MIR300* expression was up to 800-fold lower in dividing CD34$^+$ progenitors than qLSCs (CD34$^+$CFSE^{max}) from patients with CML (CP and BC), but similar in quiescent and proliferating CD34$^+$ UCB (Fig. 1B) cells.

Restoring *MIR300* expression at physiologic levels by *CpG*-based oligonucleotides (500 nmol/L *CpG-miR-300*) reduced ≥75% proliferation and clonogenic potential and enhanced apoptosis (spontaneous and TKI-induced) of CD34$^+$ CML (CP and BC), but not UCB cells (Fig. 2A and B). Importantly, Ki-67/DAPI and FUCCI2BL-mediated cell-cycle analyses in CD34$^+$ CML and LAMA-84 cells, respectively, indicated that *MIR300* arrested cell cycle and markedly expanded qLSC (G0 ≅ 50%) and apoptotic sub-G_1 cell fractions of CML, but not normal CD34$^+$ cells (Fig. 2C).

Inhibition of *MIR300* function (500 nmol/L *CpG-anti-miR-300*) did not reduce numbers [carboxyfluorescein diacetate succinimidyl diester (CFSE) assay] and clonogenic activity [colony forming cells (CFC) and/or long term culture-initiating cells (LTC-IC) of CML and normal CD34$^+$ stem and progenitor cells (Fig. 2D; Supplementary Fig. S1). In contrast,

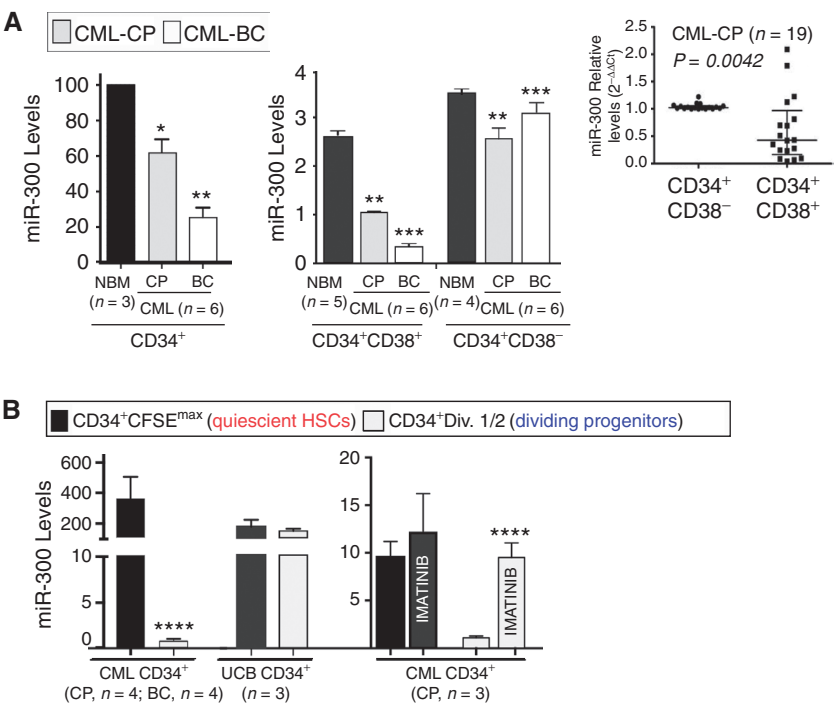

Figure 1. *MIR300* loss in leukemic progenitors and differential induction of its cell context–independent tumor suppressor activities in quiescent LSCs. **A,** (left) *MIR300* levels in healthy NBM and CML-CP and -BC CD34$^+$ BM cell fractions. Inset shows *MIR300* levels in additional CD38$^-$ fractionated CD34$^+$ CML-CP BM cells expressed as n-fold difference in CD34$^+$CD38$^+$ compared with CD34$^+$CD38$^-$ samples. **B,** *MIR300* levels in untreated and imatinib (24 hours)-treated CD34$^+$ quiescent (CFSE^{max}) and dividing (Div.1) CFSE-labeled CML and UCB cells. Asterix on CD34$^+$CD38$^-$ cell populations (panel 1a) indicate significance between *MIR300* levels CD34$^+$CD38$^-$ versus CD34$^+$CD38$^+$ cells. Data are shown as mean ± SEM from at least three independent experiments; *, $P < 0.05$; **, $P < 0.01$; ***, $P < 0.001$; ****, $P < 0.0001$.

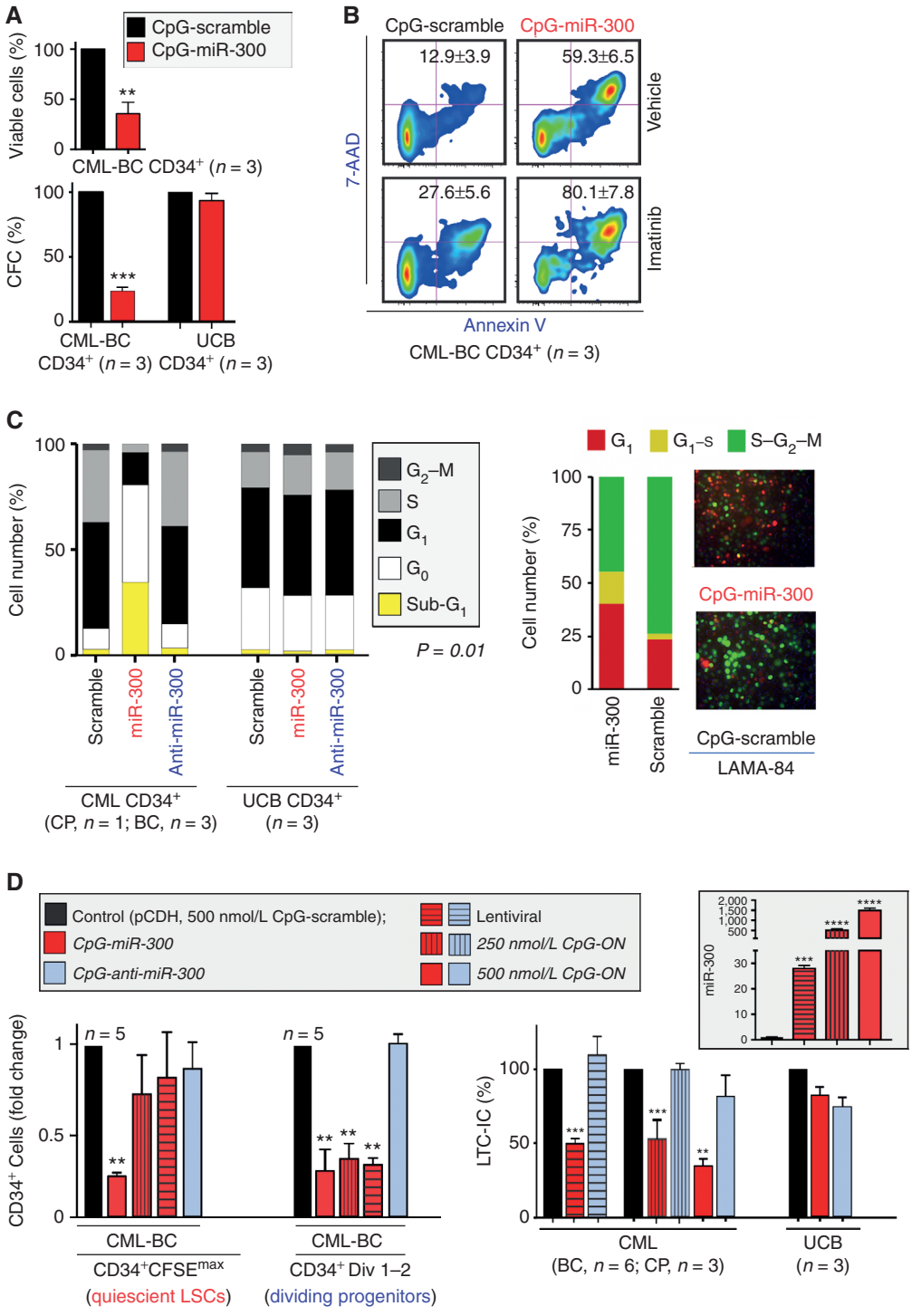

Figure 2. *MIR300* activity in quiescent leukemic stem and progenitor cells. **A,** Growth (48 hours) and clonogenic potential (CFC) of *CpG-scramble*- and *CpG-miR-300*-treated (500 nmol/L) CD34+ CML-BC and UCB cells. **B,** Effect of *CpG-miR-300* and *CpG-scramble* (500 nmol/L) on spontaneous and IM (18 hours)-induced apoptosis (Annexin V/7-AAD) in CD34+ CML-BC cells ($n = 3$). Data are reported as mean ± SE ($P < 0.01$) from three independent experiments inside representative Annexin V/7AAD FACS pseudocolor plots. **C,** Ki-67/DAPI (left; G_0: *MIR300* ≅ 46% vs. scr ≅ 10%; G1: *MIR300* ≅ 15% vs. scr ≅ 50%; S/G_2–M: *MIR300* ≅ 4% vs. scr ≅ 27.4%; and sub-G_1: *MIR300* ≅ 35% vs. scr ≅ 3%) and FUCCI-2BL (right; G_1–G_0: *MIR300* ≅ 40.2% vs. scr ≅ 23.6%; G_1–S: *MIR300* ≅ 15% vs. scr ≅ 2.85%; S/G_2–M: *MIR300* ≅ 45% vs. scr ≅ 76.6%) cell-cycle analysis of UBC and Ph+ (primary CD34+ and synchronized LAMA-84) cells exposed to the indicated *CpG-ONs*. **D,** Dose-dependent differential regulation of *MIR300* antiproliferative and proapoptotic activities on CML qLSC ($CFSE^{max}$) and progenitor (Div. 1–2) cell (left) and LTC-IC (right) numbers. Vector transduced and 500 nmol/L *CpG-scramble* and *CpG-anti-miR-300* served as controls. Inset, *MIR300* levels in *pCDH-MIR300* lentiviral–transduced and 250–500 nmol/L *CpG-miR-300*–treated Ph+ cells. Data are shown as mean ± SEM from at least three independent experiments; *, $P < 0.05$; **, $P < 0.01$; ***, $P < 0.001$; ****, $P < 0.0001$. Range values of controls are reported in Supplementary Table S1.

graded ectopic *MIR300* expression (Fig. 2D, inset) differentially affected leukemic, but not UCB-quiescent stem cell activity and survival. In fact, low *MIR300* levels (pCDH-MIR300 and 250 nmol/L *CpG-miR-300*) strongly inhibited CML (CP and BC) LTC-IC and/or CFC/replating activities without affecting qLSC numbers, whereas high *MIR300* doses (500 nmol/L *CpG-miR-300*) also reduced by more than 80% CML qLSCs and dividing $CD34^+$ progenitor cell numbers (Fig. 2D; Supplementary Fig. S1). Thus, *MIR300* functions as a cell context–independent dual activity (antiproliferative and proapoptotic) tumor suppressor that inhibits LTC-IC–driven colony formation by impairing qLSC ability to enter cycle and undergo cytokine-induced differentiation without affecting their survival, which is halted at higher *MIR300* expression levels.

MIR300 Acts as Master PP2A Activator and Inhibitor of G_1–S Transition in CML LSCs and Progenitors

Consistent with the absolute requirement of PP2A inhibition for CML, but not normal stem/progenitor cell proliferation and survival (9), gene ontology (GO) and Kyoto Encyclopedia of Genes and Genomes (KEGG) functional enrichment and clustering of *MIR300*-predicted and -validated (e.g., CTNNB1, CCND2, and Twist1; ref. 19) mRNA targets indicated that most of *MIR300* targets are also validated PP2A targets (Supplementary Fig. S2) and that *MIR300* antiproliferative and proapoptotic activities may result either from targeting SET that, in turn, induces PP2A-dependent inactivation of factors important for G_1–S cell-cycle transition (e.g., CCND2, CDK6) and survival (e.g., CTNNB1, JAK2, Twist1, and MYC) of CML qLSCs and progenitors, or from their direct inhibition by *MIR300* (Supplementary Figs. S2 and S3A). Accordingly, *CpG-miR-300*, but not *CpG-scramble*, reactivated PP2A and markedly reduced CCND2, CDK6, JAK2, hnRNPA1, SET, CTNNB1 (β-catenin), MYC, and Twist1 expression in primary $CD34^+$ CML (CP and BC) progenitors and Philadelphia-positive (Ph^+) cell lines, but not in normal $CD34^+$ cells (Fig. 3A) in which PP2A has no proapoptotic activity (8, 20). Importantly, expression of *MIR300*-insensitive Flag-tagged *SET* mRNAs lacking the entire 3′UTR (Flag-SET) or just a region encompassing the high- and low-affinity *MIR300*-binding sites (Flag-Δ3′UTR-SET), but not that of full-length wild-type SET (Flag-wt3′UTR-SET), rescued Ph^+ cells from *MIR300*-induced cell-cycle arrest and PP2A-dependent apoptosis (Annexin V^+ cells; Fig. 3A, right).

MIR300 Dual Activity Is Regulated in a Dose-Dependent Differential Target-Selection Manner

Hierarchically clustering of *MIR300* predicted and validated targets based on integration of different algorithms, some of which also take into account levels of *MIR300* and of its targets in normal and leukemic BM cells (i.e., ComiR, CSmiRTar), positioned the G_1–S cell-cycle regulators CCND2 and CDK6 within the top 2% and SET within the 5% of *MIR300* targets, followed by JAK2, hnRNPA1, CTNNB1, and Twist1 clustering within the top 25%, and MYC in the lower 75% of *MIR300*-interacting mRNAs (Fig. 3C; Supplementary Fig. S3B). Notably, other regulators of G_1–S transition (e.g., CNNA2) and LSC cell-cycle reentry (e.g., Notch signaling) clustered together with CCND2 and CDK6, whereas *MIR300* targets, belonging to JAK-STATs, PI3K-Akt, Wnt, MAPK signaling pathways, and regulating CML (CP and BC) progenitor cell survival and expansion, ranked below SET and within the bottom 75% of *MIR300* target distribution (Supplementary Fig. S3B), suggesting that their *MIR300*-induced inactivation/downregulation is PP2A-mediated, occurs upon SET inhibition, and requires levels of *MIR300* higher than those necessary to inhibit CCND2 and CDK6 and trigger cell-cycle arrest in a PP2A-independent fashion. This implies that the differential induction of *MIR300* antiproliferative and proapoptotic activities (Fig. 2C and D) may depend on its ability to select targets in a dose-dependent manner. Indeed, low levels of ectopic *MIR300* expression, achieved by exposing $CD34^+$ CML-BC stem/progenitor cells to *CpG-miR-300* concentrations (e.g., 100 nmol/L) not triggering qLSC apoptosis (Fig. 2D), strongly reduced CCND2 and CDK6, but not SET expression that, instead, became barely detectable at *CpG-miR-300* doses (e.g., 500 nmol/L) inducing qLSC apoptosis (Fig. 3B, right). This is also consistent with the presence of four, six, and two *MIR300*-binding sites in *CCND2, CDK6*, and *SET* mRNA 3′UTRs, respectively (Fig. 3B, left).

Because CDK6/CCND2 downregulation is an essential feature of G_1–G_0–arrested myeloid qLSCs (21, 22) and SET inhibition is sufficient for inducing PP2A-dependent CML LSC and progenitor cell apoptosis (8, 9), the ability of *MIR300* to sequentially trigger growth arrest and PP2A-mediated apoptosis of $CD34^+$ CML (CP and BC) qLSCs and progenitors suggests that *MIR300* expression in LSCs may account for their entry into quiescence, whereas its downregulation in leukemic progenitors likely occurs to prevent apoptosis (Fig. 3B, right).

MIR300 Antiproliferative Activity Accounts for BMM-Induced CML LSC Entry into Quiescence

MIR300 is under the control of an intergenic differentially methylated region (IG-DMR) preceding and controlling the expression of maternally expressed genomic-imprinted MEG3 lncRNA and other DLK1-DIO3 miRNAs (Supplementary Fig. S4A) that are strongly inhibited upon promoter methylation in several types of cancer, including myeloid leukemias (23). Treatment with 5-Aza-2′-deoxycytidine (5-Aza) augmented by 10^4–10^5-fold *MIR300* expression in Ph^+ cells (Supplementary Fig. S4B); however, nearly all cells underwent apoptosis after 24 hours, suggesting that *MIR300* upregulation in CML qLSCs unlikely depends on IG-DMR demethylation and expression of all 74-cluster B tumor suppressor miRNAs (Supplementary Fig. S4A). Thus, *MIR300* induction may depend on BM osteogenic niche factors (e.g., MSCs, hypoxia, TGFβ1), known to inhibit growth and induce quiescence of leukemic cells (13, 14).

Indeed, expression of *MIR300* increased at qLSC or higher levels (Fig. 1B) upon exposure of primary $CD34^+$ CML-BC and/or LAMA-84 cells and BM-derived primary $CD34^-CD45^-CD73^+CD105^+CD90^+CD44^+$ hMSCs and HS-5 MSCs to hypoxia, suggesting that MSCs may also contribute to enhanced *MIR300* levels in qLSCs (Fig. 4A and B).

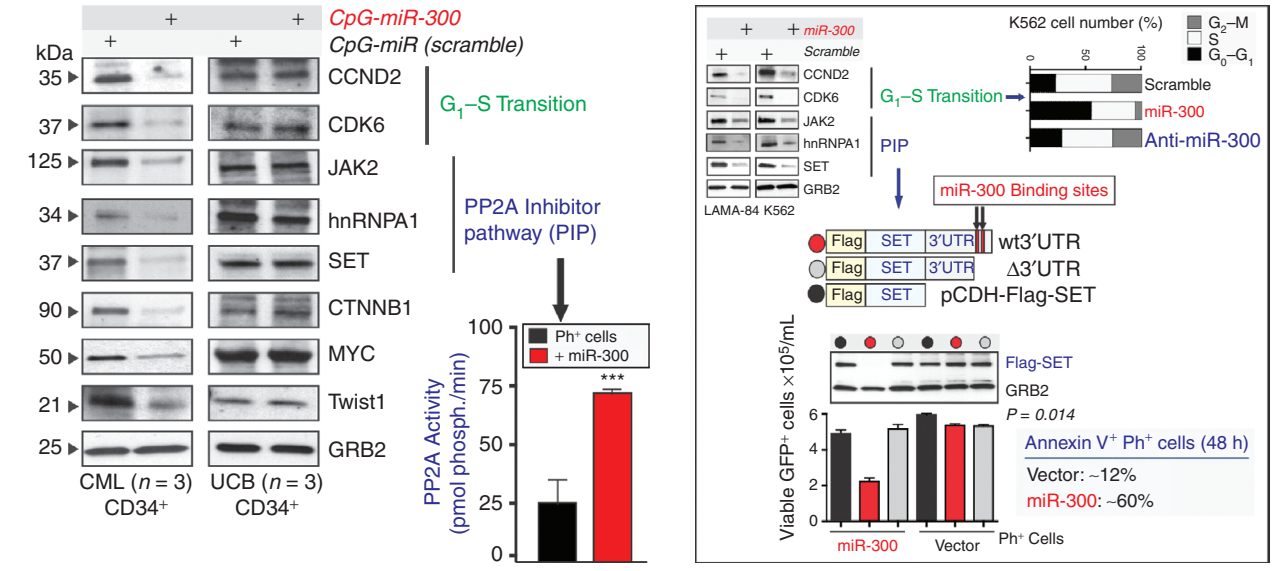

B

CONFIDENCE CLASS	
Top 1%	VERY HIGH
Top 5%	HIGH
Top 1/3	MEDIUM
Bottom 2/3	LOW

hsa-miR-300 Dose-dependent target selection

mRNA Targets (3'UTR)	DIANA microT-CDS # MRE	(length, mer)	ComiR SCORE (miRNA levels)	CSmiRTar AVN SCORE (BM levels)	mirDIP 4.1 SOURCES (30 algorithms)	Integrated score (CONFIDENCE CLASS)
CCND2	4	9(1), 6(3) mer	0.90	0.51	12	0.63
CDK6	6	3(7), 6(3) mer	0.89	0.42	9	0.62
SET	2	8, 6 mer	0.84	0.33	14	0.53
JAK2	6	9(1), 7(2) mer	0.83	0.30	14	0.46
TWIST1	1	6 mer	0.84	0.27	10	0.52
hnRNPA1	2	7 mer	0.83	0.27	11	0.51
CTNNB1	1	7 mer	0.83	0.30	12	0.47
MYC	1	6 mer	0.23	0.14	6	0.19

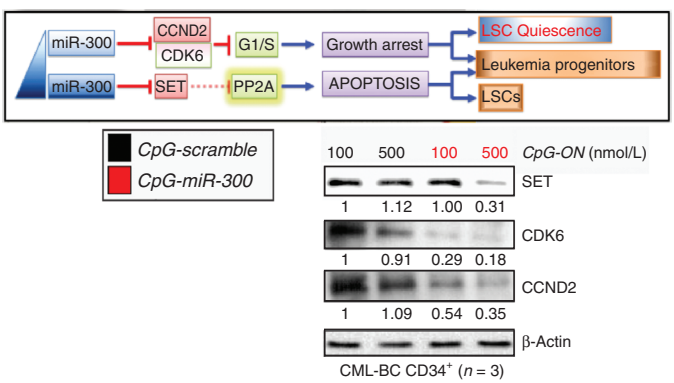

Figure 3. *MIR300* acts as master PP2A activator and inhibitor of G_1–S transition through a dose-dependent target selection mechanism. **A,** Left:, representative blots show effect of *MIR300* on its targets and PP2A activity in UCB and CML-BC CD34+ cells and cell lines exposed to *CpG-scramble* and *CpG-miR-300* (500 nmol/L; 48–72 hours). Right, (top) Dapi/Ki67 cell-cycle analysis of *CpG-scramble*, *-miR-300*, and *CpG-anti-miR-300* (500 nmol/L; 21 hours)-treated aphidicolin-synchronized K562 cells; (middle) Flag-SET lentiviral constructs with wild-type or a deleted mRNA 3′UTR; (bottom) *MIR300*-induced downregulation of Flag-SET proteins, and rescue of Ph+ cells from exogenous *MIR300*-induced growth inhibition (Trypan blue exclusion)/apoptosis (Annexin V+) by Flag-SET cDNAs lacking *MIR300*-binding site. Similar results were obtained with LAMA-84 cells. **B,** Hierarchical clustering of statistically significant ($P < 0.05$ with FDR correction) *MIR300* targets using the indicated databases (number of binding sites is indicated in red). Top right, schematic representation of the biological effects of *MIR300* dose-dependent target selection activity in qLSCs and leukemic progenitors; (bottom) SET, CDK6, CCND2, and β-actin levels in *CpG-MIR300*- and *CpG*-scramble–treated (100–500 nmol/L; 48 hours) CML-BC CD34+ cells.

Accordingly, *MIR300* expression was strongly augmented in CD34+ CML cells exposed to hMSC and HS-5 conditioned medium (CM) and/or *MIR300*-containing CD63+Alix+ MSC exosomes (100 μg/mL; Fig. 4C).

Hypoxia- and MSC-induced *MIR300* expression correlated with 40% to 60% reduced cell division and, importantly, with doubled numbers of cells in the $CFSE^{max}$ CD34+ qLSC compartment (Fig. 4B and C; Supplementary Fig. S4C). Ph+ LAMA-84 cells also responded to MSC-CM exposure by ceasing proliferation and modifying gene expression (Supplementary Fig. S4D, left and right) in a manner similar to that of CML qLSCs (1). Importantly, exposure to MSCs (CM and/or exosomes) neither diminished SET and $PP2Ac^{Y307}$ (inactive) levels (Supplementary Fig. S4D, right) nor induced cell death (unchanged cell viability), suggesting that MSCs increase *MIR300* expression in CD34+ LSCs at levels sufficient to induce cell-cycle exit, but not to trigger PP2A-mediated apoptosis. Moreover, anti-*MIR300* molecules (*pZIP-miR-300* or *CpG-anti-miR-300*) suppressed hypoxia-induced *MIR300* target downregulation in CD34+ CML stem/progenitor cells and prevented MSC-induced inhibition of their proliferation when expressed in MSCs (Fig. 4A and C), further indicating that *MIR300* antiproliferative activity likely mediates BMM-induced CD34+ LSC entry into quiescence in CML (CP and BC). Note that increased

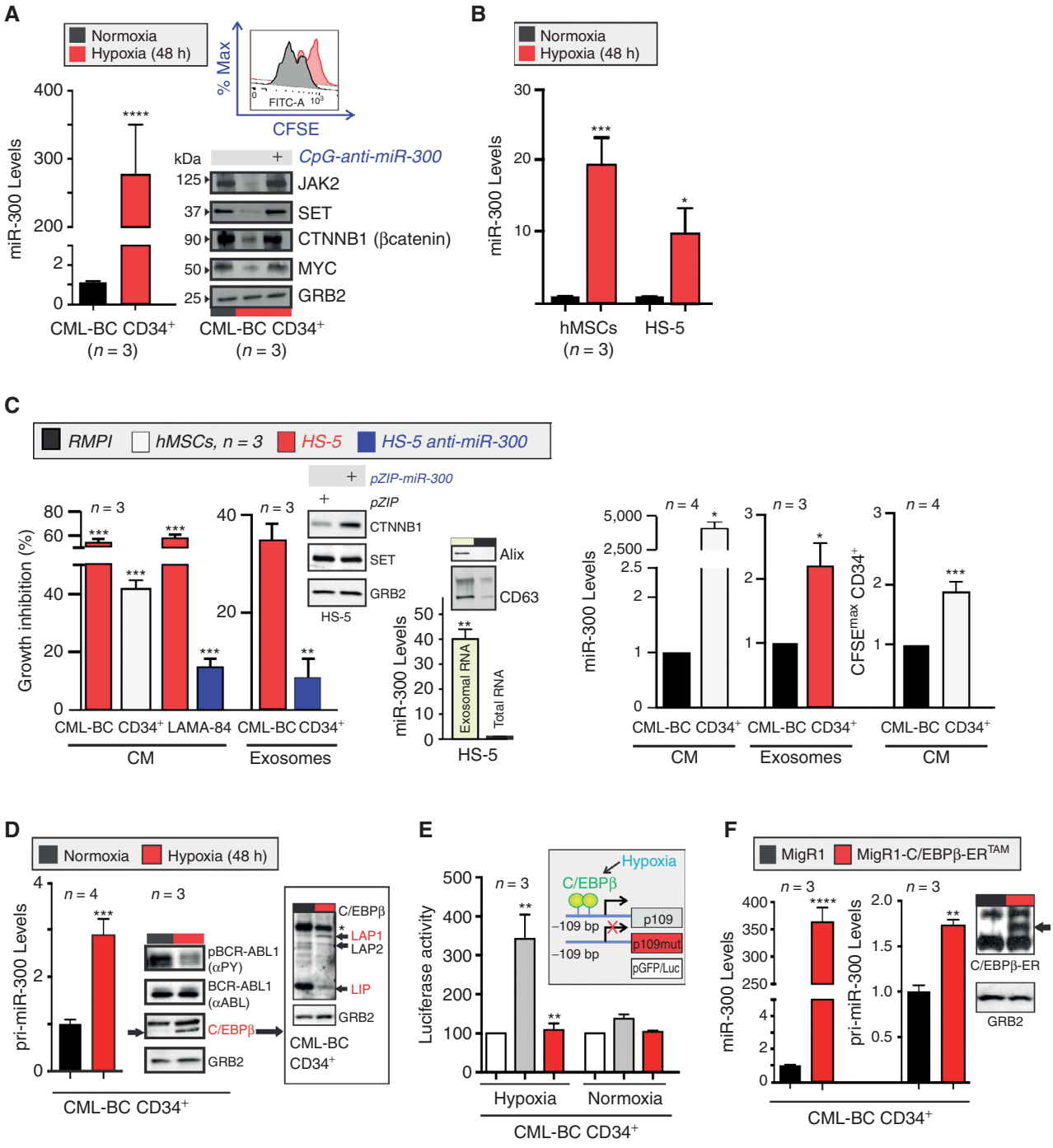

Figure 4. C/EBPβ-dependent *MIR300* tumor suppressor antiproliferative activity accounts for BMM-induced LSC entry into quiescence. **A,** Effect of hypoxia on (i) *MIR300* levels in CD34+ CML-BC, and BM-derived primary (hMSCs) and HS-5 MSCs (**B**); and (ii) *MIR300* targets in untreated and *CpG-anti-miR-300*–treated (500 nmol/L, 48 hours) and CML-BC cells. Inset, effect of hypoxia on CFSE+CD34+ CML-BC proliferation. **C,** Effect of hMSC and HS-5 conditioned medium (CM) and/or exosomes (50–100 μg/mL) from parental, vector (pZIP), and anti-*MIR300* (pZIP-*MIR300*)–transduced primary hMSCs and/or HS-5 cells on: (i) proliferation (% growth inhibition); (ii) qLSC fraction ($CFSE^{max}CD34^+$); and (iii) *MIR300* levels in CD34+ CML-BC and LAMA-84 cells. Insets, β-catenin and SET levels in anti-*MIR300* (*pZip-300*)–transduced HS-5 (left); *MIR300* in HS-5 Alix+CD63+ exosomes (right). **D,** Effect of hypoxia on primary *MIR300* transcripts (*pri-miR-300*), C/EBPβ (LAP1, LAP2, and LIP isoforms), BCR-ABL1 expression (αABL) and activity (αPY), and GRB2 levels in CD34+ CML-BC cells. (*): nonspecific band. **E,** *MIR300* promoter/enhancer activity in hypoxia- (48 hours) and normoxia-cultured CML-BC CD34+ cells transduced with pGFP/Luc-based *MIR300*-reported constructs. p109mut is mutated in the -64 and -46 bp C/EBPβ-binding sites. **F,** Effect of ectopic C/EBPβ (inset) on mature (*MIR300*) and primary (*pri-miR-300*) *MIR300* levels in CD34+ CML-BC cells. Data are represented as mean ± SEM for at least three experiments. Range values of controls are reported in Supplementary Table S1.

β-catenin in HS-5 cells indicated functionality of lentivirally-transduced anti-*MIR300* construct (Fig. 4C, inset).

Hypoxia-Induced *MIR300* Expression in CML-BC LSCs Requires C/EBPβ Activity

The notion that hypoxia induces quiescence of CD34$^+$ CML LSCs and progenitors (24), and that hypoxia, but not MSCs, induces *MIR300*-dependent SET inhibition and increases levels of mature and primary (pri-miR-300) *MIR300* transcripts (Fig. 4A and D; Supplementary Fig. S4D) suggests that the contribution of hypoxia to *MIR300* expression in qLSCs is greater than that of MSC-derived exosomes, and that it may depend on increased *MIR300* transcription. Indeed, luciferase (luc) assays in normoxia- and hypoxia-cultured CD34$^+$ CML-BC stem/progenitor cells transduced with reporter constructs containing full-length or 5′-deleted *MIR300* intergenic region revealed the presence of a hypoxia-sensitive regulatory element in the 109 bp preceding the human *MIR300* gene (Fig. 4E). ENCODE (V3) ChIP-Seq and PROMO analyses revealed that this 109 bp is located in a DNaseI hypersensitive region and contains two CCAAT Enhancer Binding Protein B (C/EBPβ)-binding sites at position −64 and −46 that may drive transactivation of *MIR300* transcription. Site-directed mutagenesis of these C/EBPβ-binding sites (p109mut) resulted in loss of luc activity (Fig. 4E), indicating that C/EBPβ binding to this 109 bp regulatory element is essential for *MIR300* transactivation in hypoxia-, but not normoxia-cultured CD34$^+$ CML-BC cells. Accordingly, increased pri-miR-300 expression correlated with markedly higher C/EBPβ LAP1 (transcriptionally active) levels in hypoxic CD34$^+$ CML-BC cells (Fig. 4D). In contrast, lack of C/EBPβ-driven p109-luc activity in normoxic CD34$^+$ CML-BC progenitors correlated with increased C/EBPβ LIP (inhibitory function) expression (Fig. 4D). Consistent with the notion that *CEBPB* translation is inhibited by BCR-ABL1 activity (25) and that hypoxia inactivates BCR-ABL1 to induce LSC quiescence (14), *MIR300* induction by hypoxia was associated with decreased BCR-ABL1 activity, but not expression, (Fig. 4D) and ectopic C/EBPβ-ER^{TAM} expression rescued primary (pri-miR-300) and mature *MIR300* expression in normoxic CD34$^+$ CML-BC cells (Fig. 4F).

Hypoxia also substantially increased by 10- to 20-fold *MIR300* and C/EBPβ protein, but not mRNA levels, in BM-derived primary MSCs and/or HS-5 cells (Fig. 4B; Supplementary Fig. S4E), suggesting that the hypoxic conditions of the osteogenic BM niche may increase *MIR300* levels in CML LSCs by simultaneously inducing C/EBPβ LAP1-dependent *MIR300* transcription and increasing transfer of MSC-derived exosomal *MIR300*. Conversely, the evidence showing that *MIR300* levels in C/EBPβ–responsive CD34$^+$ CML-BC cells and/or Ph$^+$ cell lines were not influenced by ectopic C/EBPα expression or exposure to TGFβ1-blocking antibody (Supplementary Fig. S4F and S4G), indicated that these qLSC regulators do not contribute to increased *MIR300* expression.

Notably, the notion that mouse c/ebpβ induces BCR-ABL$^+$ LSK exhaustion (26) does not argue against a role for human C/EBPβ as an inducer of LSC quiescence because: (i) LSKs are pushed into cycle by constitutively activated BCR-ABL1 that promotes C/EBPβ-dependent LSK maturation (26), (ii) the hypoxia-sensitive C/EBPβ-responsive *MIR300* regulatory element is not conserved in mouse cells, and (iii) an A-to-G substitution in mmu-miR-300 seed sequence at +4 position is predicted (miRTar, MFE: ≤ −10 kcal/mol; score: ≥136.5) to prevent mouse *MIR300* targeting of *ccnd2* and *cdk6* mRNAs.

MIR300 Is Upregulated in CML NK Cells and Its BMM-Induced Antiproliferative and PP2A-Activating Functions Impair NK Cell Immune Response

In CML, loss of NK cell antitumor immune response is causally linked to persistence of TKI-resistant LSCs (4, 27, 28). Cytotoxicity assays showed that cytokine-activated CD56$^+$CD3$^-$ NK cells can kill CD34$^+$ CML-initiating qLSCs (Fig. 5A). Because cytokine-induced CCND2 expression and SET-dependent PP2A inhibition are essential for CD56$^+$CD3$^-$ primary NK and clinically relevant NK-92 cell proliferation and antitumor cytotoxicity (refs. 29, 30; Supplementary Fig. S5A), and KEGG/GO analyses predicted that *MIR300* regulates innate anticancer immunity (Supplementary Fig. S3A, right), we assessed whether reduced numbers and dysfunctional NK cells in patients with CML (28, 31) depend on increased *MIR300* expression.

MIR300 levels were increased in CD56$^+$CD3$^-$ NK cells from patients with CML at diagnosis, but not in NK cells, from healthy individuals (Fig. 5B), suggesting that loss of NK-cell proliferation and killing activity against CD34$^+$ CML qLSCs and progenitors may depend on BMM-generated and leukemia-sustained *MIR300* antiproliferative and PP2A-activating functions. Indeed, exposure to hypoxia and BM MSC (primary hMSCs and HS-5 cells)-derived CM and/or Alix$^+$CD63$^+$ exosomes reduced by 45% to 75% IL2-dependent proliferation of CD56$^+$CD3$^-$ primary NK and NK-92 cells (Fig. 5C and D; Supplementary Fig. S5B) and severely impaired NK-cell immunoregulatory (IFNγ production) and anticancer cytotoxic (K562 killing) activities (Fig. 5E). Importantly, lentiviral anti-miR-300 (pZIP-miR-300) transduction into HS-5 cells and pretreatment of NK-92 cells with *CpG-anti-miR-300*, but not with *CpG-scramble*, significantly suppressed MSC CM- and/or exosome-inhibitory effects on NK cell proliferation and cytotoxicity against CML cells (Fig. 5D and E). Accordingly, IL2-induced proliferation and cytotoxicity of CD56$^+$CD3$^-$ NK and clinically relevant NK-92 cells was suppressed in *CpG-miR-300*-, but not *CpG-scramble*–treated cells (Fig. 5F), suggesting that impaired NK-cell growth and cytotoxicity against CML qLSCs and proliferating blasts occur in a *MIR300*-dependent manner through hypoxia- and MSC-(CM and exosomes) generated signals, increasing levels of C/EBPβ and *MIR300* that, in turn, reduces CCND2, CDK6, and SET expression (Fig. 5C, E, and F).

Selective Suppression of *MIR300* Proapoptotic, But Not Antiproliferative Activity by *TUG1* lncRNA in CML Quiescent LSCs

Myeloid qLSCs display low to undetectable CCND2 and CDK6 expression, but high SET levels (9, 22, 32), and survive despite the high expression levels of a functional (target downregulation) *MIR300* (Figs. 1B and 4A), suggesting that a *MIR300*-interacting factor differentially regulates *MIR300* activities to prevent CML qLSC apoptosis while allowing LSC cell-cycle exit.

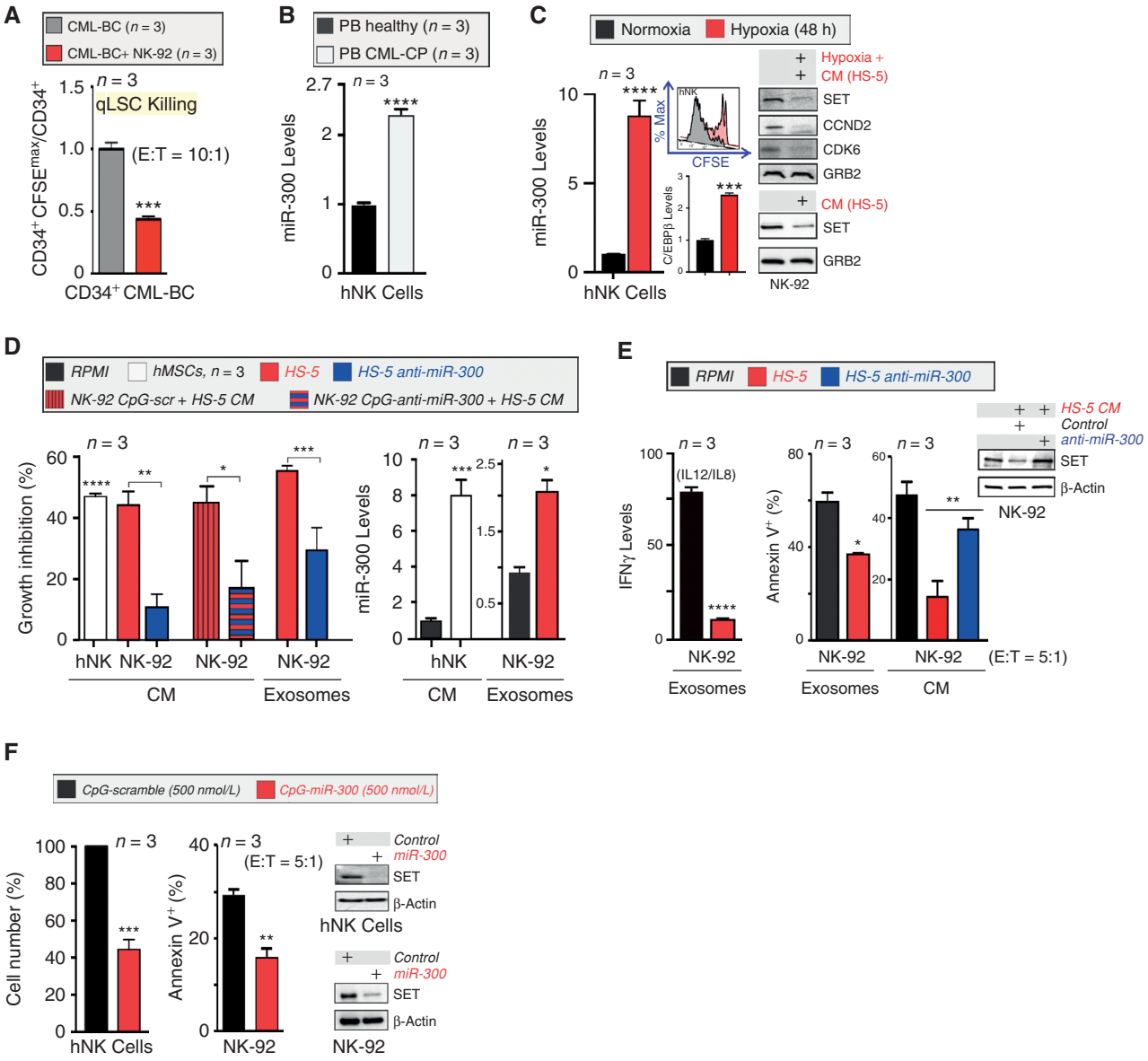

Figure 5. BMM-induced *MIR300* antiproliferative and PP2A-activating functions impair NK cell immune response. **A,** NK-92 cell cytotoxicity against CML-BC qLSCs. **B,** *MIR300* levels in $CD56^+CD3^-$ NK (hNK) cells from healthy and CML-CP individuals. **C,** Effect of hypoxia and MSC CM on *MIR300*, C/EBPβ, SET, CCND2, CDK6, and GRB2 levels in hNK and/or NK-92 cells. Inset, effect of hypoxia on $CFSE^+$ NK cell growth. **D,** Effect of CM and exosomes from hMSCs and from parental, vector-, and anti-*MIR300*–transduced HS-5 cells on proliferation (left) and *MIR300* levels (right) in hNK and untreated, 500 nmol/L *CpG-scramble* or *CpG-anti-MIR300*–treated NK-92 cells. **E,** IL12/IL18 (18 hours)-induced IFNγ mRNA levels and NK cytotoxicity (% Annexin V^+ K562 cells) in IL2-cultured NK-92 cells exposed to CM or exosomes from parental or vector- and anti-*MIR300*–transduced HS-5 cells. Inset, SET and actin levels in NK-92 exposed to vector- and anti-miR300–transduced HS-5 CM. RPMI medium served as control. **F,** Effect of *CpG-scramble* and *CpG-miR-300* treatment (500 nmol/L; 36 hours and 7 days) on IL2-depleted NK-92 cytotoxicity (% Annexin V^+ K562 cells), IL2-induced hNK cell proliferation (% cell number), and on SET and β-actin expression. Data are represented as mean ± SEM for at least three experiments. Range values of controls are reported in Supplementary Table S1.

Because the taurine upregulated gene 1 (*TUG1*) is a *MIR300*-interacting (33) long noncoding RNA (lncRNA) that prevents the inhibition of *MIR300*-regulated factors (e.g., CCND1, CTNNB1, and Twist1) described as important for tumor cell growth and survival (34), we investigated whether *TUG1* may differentially regulate *MIR300* tumor suppressor activities in CML qLSCs (Fig. 6A).

TUG1 levels are markedly increased in $CD34^+CFSE^{max}$ CML qLSCs compared with dividing $CD34^+$ CML progenitors and to $CD34^+CFSE^{max}$ UCB cells, but not in either $CD34^+CFSE^{max}$ UCB HSCs, compared with dividing $CD34^+$ UCB progenitors or $CD34^+$ Lin^- compared with $CD34^+$ Lin^+ BM cells from healthy individuals (Fig. 6B; Supplementary Fig. S6A and S6B). In CML, *TUG1* is regulated in a manner similar to that of *MIR300*; in fact, *TUG1* expression is imatinib-insensitive in qLSCs, but not in dividing $CD34^+$ progenitors in which it is markedly suppressed by BCR-ABL1 activity (Fig. 6B).

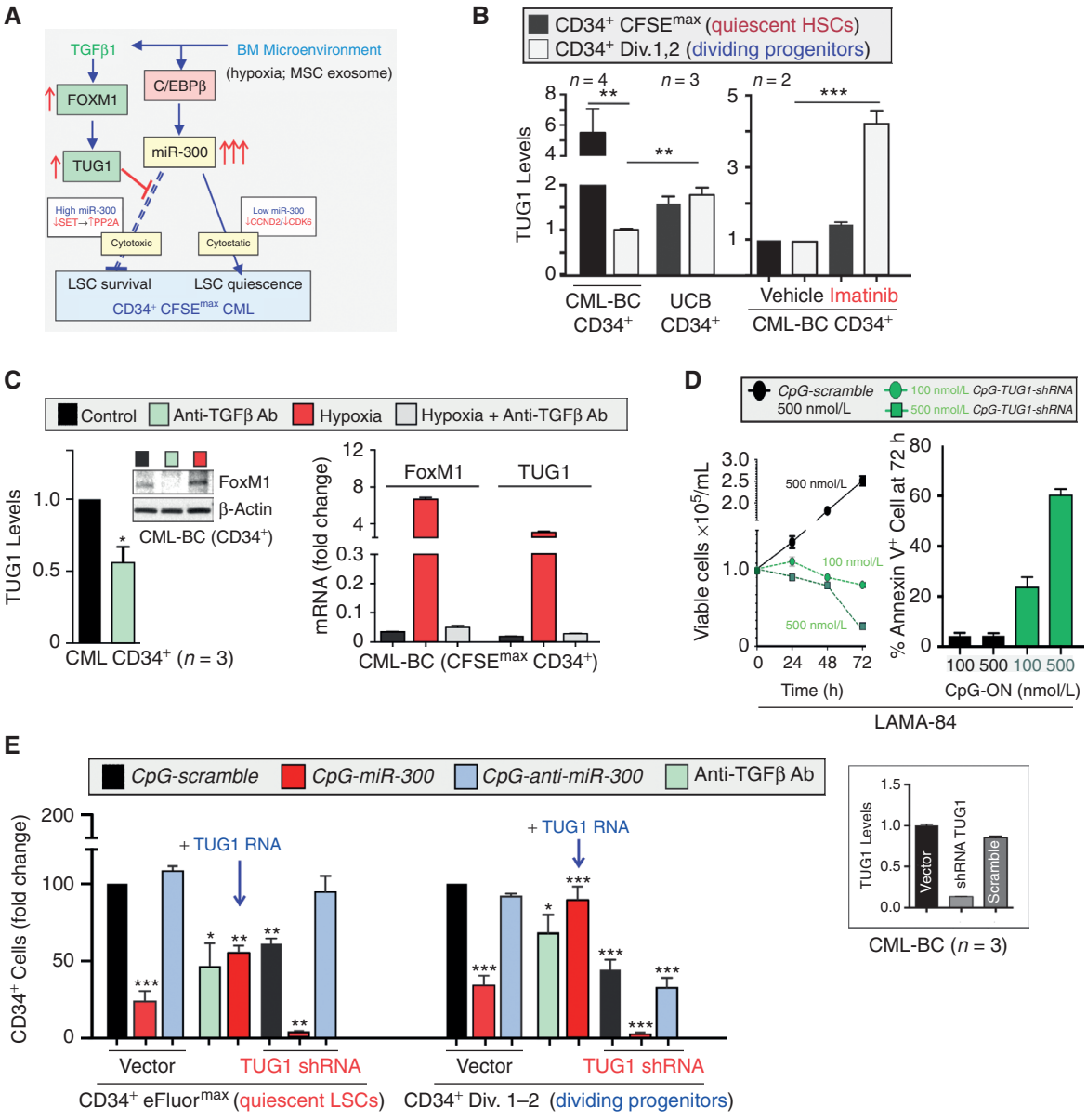

Figure 6. Selective suppression of *MIR300* proapoptotic, but not antiproliferative, activity by *TUG1* lncRNA in CML quiescent LSCs. **A,** BMM-generated signals regulating *MIR300-TUG1* interplay and its effect on CML LSC survival and quiescence. **B,** *TUG1* levels in CD34+ quiescent stem ($CFSE^{max}$) and dividing progenitors (Div.1, 2) and in untreated and imatinib-treated CD34+ CML cells. **C,** Effect of anti-TGFβ antibody (Ab) and/or hypoxia (1% O_2, 48 hours) on *TUG1* lncRNA and FoxM1 levels in CD34+ and $CD34^+CFSE^{max}$ CML-BC cells. **D,** Dose-dependent differential effect of low (100 nmol/L) and high (500 nmol/L) *CpG-TUG1-shRNA* and *CpG-scramble* on Ph^+ LAMA-84 cell proliferation and survival (Annexin V). **E,** Effect of anti-TGFβ Ab, *TUG1*-shRNA, *TUG1* RNA, and control (*CpG*-scramble or empty vector) on recovery of untreated and *CpG-scramble*, *-miR-300*, and/or *-anti-miR-300* eFluor+CD34+ CML qLSCs ($eFluor^{max}$) and dividing (Div.1-2) progenitors relative to input. *Inset*, *TUG1* levels in vector, *TUG1 shRNA* and scramble-shRNA cells. Data are represented as mean ± SEM for at least three experiments. Range values of controls are reported in Supplementary Table S1.

Because *TUG1* expression correlates with that of TGFβ1 in tumor cells (35) and TGFβ1 is a known inducer of LSC quiescence and it is secreted by leukemic cells including CD34+ CML blasts (36), we investigated the role of TGFβ1 in the regulation of *TUG1* expression and activity in CD34+ CML qLSCs and progenitors. Exposure (48 hours) of CD34+ CML-BC cells to a TGFβ1-blocking antibody (anti-TGFβ Ab; green bars) halves *TUG1* levels and also reduces levels of FoxM1 (Fig. 6C, left), a transcriptional factor that is essential for quiescence and maintenance of hematopoietic stem cells, including CML LSCs, and induces *TUG1* expression in osteosarcoma cells (37–39). In contrast, FoxM1 and/or *TUG1* expression is strongly induced in a TGFβ-dependent manner in hypoxia-cultured (48 hours, 1% O_2) CML-BC $CD34^+CFSE^{max}$ and bulk CD34+ cells (Fig. 6C), suggesting that hypoxia-induced TGFβ1 (36) enhances *TUG1* levels in a FoxM1-dependent manner to neutralize *MIR300* proapoptotic activity in CML CD34+ qLSCs.

Indeed, dosing *TUG1* downregulation by exposure to low and high *CpG-TUG1–shRNA* concentrations mimicked the dose-dependent differential activation of *MIR300* antiproliferative and proapoptotic functions exerted by different *CpG-miR-300* doses (Fig. 2D); in fact, exposure of Ph$^+$ cells (LAMA-84) to 100 nmol/L *CpG-TUG1-shRNA* efficiently induced growth arrest, but modestly affected survival (Annexin V$^+$ cells; Fig. 6D and E, inset). Conversely, 500 nmol/L *CpG-TUG1-shRNA* decreased CD34$^+$eFluor^{max} CML-BC qLSC and LAMA-84 cell numbers in a *MIR300*-sensitive manner and further enhanced *CpG-miR-300*–driven apoptosis resulting in a nearly complete loss of CD34$^+$eFluor^{max} qLSCs and dividing CD34$^+$ leukemic progenitors (Fig. 6D and E). As expected, exposure (48 hours) to a TGFβ1-blocking antibody markedly decreases qLSC numbers, but very modestly affects dividing leukemic progenitors (Fig. 6E). In contrast, *TUG1* overexpression (*TUG1 RNA*) antagonized *CpG-miR-300*–induced qLSC and progenitor cell apoptosis (Fig. 6E). *CpG-anti-miR-300* fully prevented *TUG1-shRNA*-induced apoptosis of CML CD34$^+$eFluor qLSCs (Fig. 6E), suggesting that CML LSC entry into quiescence and qLSC survival are *MIR300*-driven *TUG1*-regulated effects. Thus, hypoxia-induced TGFβ1-FoxM1–mediated signals increase *TUG1* expression to allow CD34$^+$ CML LSC entry into quiescence and qLSC survival by maintaining the amount of free functional *MIR300* at levels sufficient for arresting cell cycle, but not for triggering PP2A-dependent apoptosis (Fig. 6A; Supplementary Fig. S6C). Conversely, *CpG-anti-miR-300* did not counteract *TUG1*-shRNA–induced apoptosis in CD34$^+$ CML progenitors (Fig. 6E). Moreover, the nearly complete killing of CD34$^+$ CML dividing progenitors induced by *CpG-miR-300* and *-TUG1-shRNA* combined treatment (Fig. 6E) suggests that the BCR-ABL1–regulated low *TUG1* expression in CD34$^+$ CML blasts (Fig. 6B) is required for inhibiting the activity of other miRNAs negatively regulating cell survival.

Disruption of *MIR300-TUG1* Interplay and PAD Treatment Abrogate the BMM-Protective Effect on Survival of CML qLSCs and BCR-ABL1$^+$ Leukemia-Initiating Cells

By using a previously described patient-derived xenograft (PDX)-based approach suitable for determining changes in CML LT-HSC survival (40), we assessed the effects of disrupting the *MIR300-TUG1* interplay on BM-repopulating CML qLSCs. NRG-SGM3 mice (n = 4/group) were transplanted with >95% Ph$^+$ CD34$^+$ CML-CP, - AP (accelerated phase) and -BC cells previously exposed for 48 hours to 500 nmol/L *CpG-scramble* (control), *CpG-miR-300*, and *CpG-TUG1-shRNA* used as single agents or in combination (Fig. 7A). At 4 and 8 weeks after engraftment, BM hCD45$^+$CD34$^+$ progenitors and LSC-enriched hCD45$^+$CD34$^+$CD38$^-$ cells were reduced by 75% to 97% in all arms (Fig. 7B and C). Inhibition and/or saturation of *TUG1 MIR300*–sponging activity with *CpG-TUG1-shRNA* and *CpG-miR-300* resulted in the killing of approximately 100% of leukemia-initiating (hCD45$^+$CD34$^+$CD38$^-$CD90$^+$) quiescent HSCs (Fig. 7C), barely detectable *BCR-ABL1* transcripts, and 3.6-fold increased numbers of normal (Ph$^-$) BM cells (Fig. 7D), and strongly reduced numbers of PB and BM CML (CP, AP and BC) hCD45$^+$ cells (Fig. 7E). Thus, *CpG*-oligonucleotide–mediated pharmacologic disruption of *MIR300-TUG1* balance allows PP2A-mediated *MIR300* proapoptotic activity to suppress chronic and blastic CML development by selectively and efficiently eliminating nearly all TKI-resistant leukemic, but not normal quiescent HSCs and progenitors. Note that the extremely low numbers (0%–0.0015% of total BM cells recovered/12 mice/arm) of *CpG-miR-300-*, *CpG-TUG1-shRNA-*, and *CpG-miR-300/TUG1-shRNA*–treated CD34$^+$CD38$^-$CD90$^+$ CML (CP, AP, and BC) BM-repopulating cells (Fig. 7C) did not justify serial BM transplantation into secondary and tertiary recipients.

Consistent with the role of *MIR300* as a BMM-induced tumor suppressor capable of triggering CML CD34$^+$ qLSC apoptosis through suppression of SET-mediated PP2A inhibition, and with the notion that SET expression is increased in CD34$^+$CD38$^-$CD90$^+$ CML LSCs (9) and that SET-sequestering PADs selectively induce apoptosis of TKI-resistant serially transplantable leukemic LT-HSCs and CD34$^+$CFSE^{max} quiescent CML, but not normal HSCs (9), PAD treatment (2 μmol/L FTY720) of HS-5-cocultured CFSE$^+$CD34$^+$ CML-BC cells markedly reduced the cobblestone area–forming cell (CAFC) activity (Fig. 7F, left) and numbers of adherent CFSE^{max}AnnexinV^{neg}CD34$^+$ CML qLSCs (~91.1% inhibition relative to DMSO-treated controls; Fig. 7F, right), suggesting that FTY720-mediated PP2A activation (20) circumvents the MSC-mediated protective effect on CML qLSC survival. Likewise, HS-5 CM did not protect LAMA-84 CML progenitors from FTY720-induced apoptosis (Supplementary Fig. S4D, middle). As expected (41), TKI treatment (imatinib) did not reduce, but augmented CAFC and qLSC numbers (Fig. 7F). Accordingly, FTY720, but not imatinib, strongly decreased CAFC activity (red arrows) derived from Lin$^-$Sca$^+$ CD45$^-$CD31$^+$CD51$^+$ mouse MSC (mMSC)-induced (inset) CFSE^{bright} 32D-BCR-ABL cells (Fig. 7G), further indicating that pharmacologic PP2A activation by SET-sequestering PADs can lead to CML eradication at qLSC level.

Figure 7. Disruption of *MIR300-TUG1* interplay and PAD treatment abrogate the BMM-protective effect on survival of CML qLSCs and BCR-ABL1$^+$ leukemia-initiating cells. **A,** Xenotransplantation protocol of *ex vivo*–treated CD34$^+$ chronic (CP), accelerated (AP) and blastic phase (BC) CML cells in NRG-SGM3 mice (n = 4 mice/treatment/patient sample). **B** and **C,** Analysis of *CpG-MIR300-*, *CpG-TUG1-shRNA-*, *CpG-TUG1-shRNA+CpG-MIR300-*, and *CpG-scramble*–treated CML cells from BM aspirates at 2–12 (3D plots) and 10 to 20 weeks posttransplant quantitative analysis of CML cells stained with the indicated antibodies. **D,** Evaluation at 10 to 20 weeks posttransplant of BCR-ABL1 transcripts by qRT-PCR (left) and of % Ph-negative (Ph$^-$) cells by FISH (right) in total and FACS-sorted hCD45$^+$BM cells, respectively. **E,** Analyses of BM CML cells at 10 to 20 weeks posttransplant: hCD45$^+$ cells (%) in BM (left) and PB (right) of mice transplanted with CML (CP, AP, and BC) and treated with the indicated *CpG-ODNs*. Age-matched mice served as controls. Error bars, mean ± SEM. **F,** Effect of 2.5 μmol/L FTY720 or 1 μmol/L imatinib (IM) on CAFC activity (left) and numbers of CFSE^{max}AnnexinV^{neg}hCD45$^+$CD34$^+$ CML qLSCs derived from CFSE-labeled CD34$^+$ CML-BC cells cocultured for 7 days on BM-derived HS-5 MSC cells (right). Inset, FACS plot shows gating of CFSE^{max} CML qLSCs. **G,** Relative number and representative images of CAFC (red arrows) of CFSE-labeled 32D-BCR-ABL cells cocultured with primary mMSCs in the absence or presence of IM (1 μmol/L, 48 hours) or FTY720 (2 μmol/L, 48 hours; n = 5). Inset: CFSE^{bright} fraction of adherent 32D-BCR-ABL cells in medium and cocultured for 4 days with mMSCs. Range values of controls are reported in Supplementary Table S1.

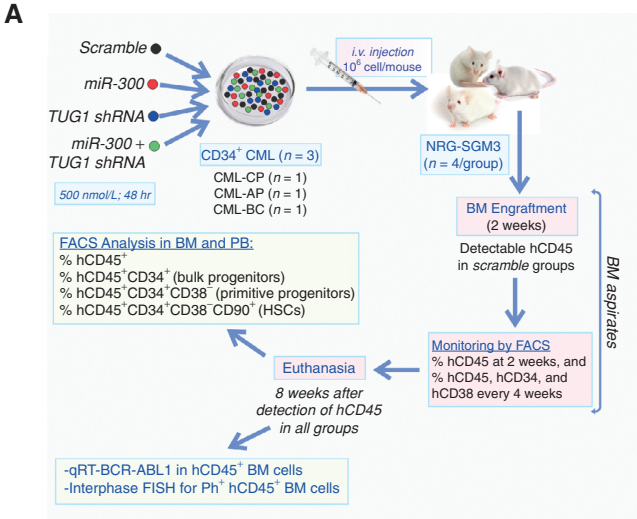
A
Scramble
miR-300
TUG1 shRNA
miR-300 + TUG1 shRNA
500 nmol/L; 48 hr
i.v. injection 10^6 cell/mouse
CD34+ CML (n = 3)
CML-CP (n = 1)
CML-AP (n = 1)
CML-BC (n = 1)
NRG-SGM3 (n = 4/group)
BM Engraftment (2 weeks)
Detectable hCD45 in scramble groups
BM aspirates
FACS Analysis in BM and PB:
% hCD45+
% hCD45+CD34+ (bulk progenitors)
% hCD45+CD34+CD38− (primitive progenitors)
% hCD45+CD34+CD38−CD90+ (HSCs)
Monitoring by FACS
% hCD45 at 2 weeks, and
% hCD45, hCD34, and
hCD38 every 4 weeks
Euthanasia
8 weeks after detection of hCD45 in all groups
-qRT-BCR-ABL1 in hCD45+ BM cells
-Interphase FISH for Ph+ hCD45+ BM cells

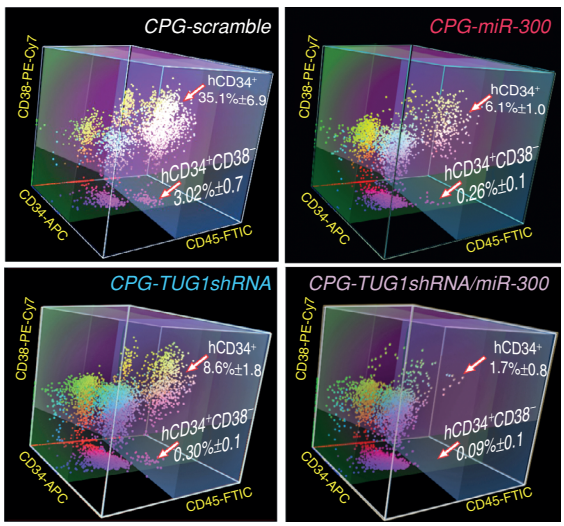
B
CPG-scramble
CPG-miR-300
CPG-TUG1shRNA
CPG-TUG1shRNA/miR-300
CD38-PE-Cy7
CD34-APC
CD45-FTIC
hCD34+ 35.1%±6.9
hCD34+CD38− 3.02%±0.7
hCD34+ 6.1%±1.0
hCD34+CD38− 0.26%±0.1
hCD34+ 8.6%±1.8
hCD34+CD38− 0.30%±0.1
hCD34+ 1.7%±0.8
hCD34+CD38− 0.09%±0.1

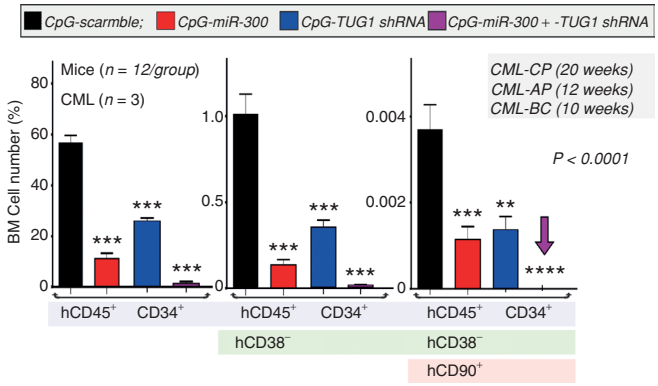
C
CpG-scramble; CpG-miR-300 CpG-TUG1 shRNA CpG-miR-300 + -TUG1 shRNA
Mice (n = 12/group)
CML (n = 3)
CML-CP (20 weeks)
CML-AP (12 weeks)
CML-BC (10 weeks)
P < 0.0001
BM Cell number (%)
hCD45+ CD34+
hCD38−
hCD90+

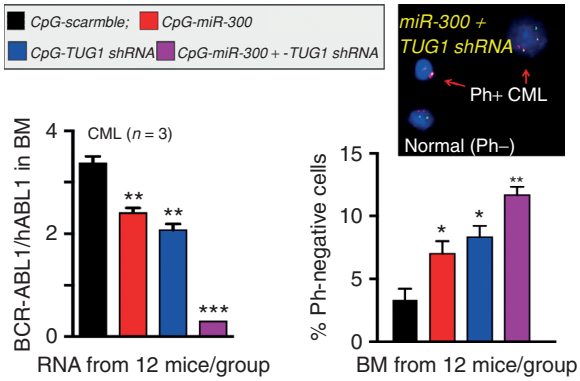
D
CpG-scramble; CpG-miR-300
CpG-TUG1 shRNA CpG-miR-300 + -TUG1 shRNA
miR-300 + TUG1 shRNA
Ph+ CML
Normal (Ph–)
CML (n = 3)
BCR-ABL1/hABL1 in BM
RNA from 12 mice/group
% Ph-negative cells
BM from 12 mice/group

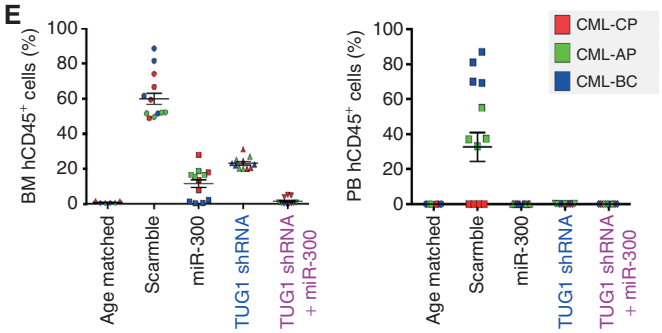
E
BM hCD45+ cells (%)
PB hCD45+ cells (%)
CML-CP
CML-AP
CML-BC
Age matched
Scramble
miR-300
TUG1 shRNA
TUG1 shRNA + miR-300

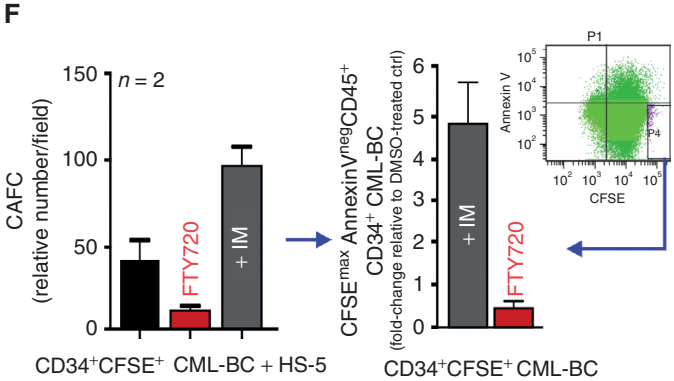
F
n = 2
CAFC (relative number/field)
FTY720
+ IM
CD34+CFSE+ CML-BC + HS-5
CFSEmax AnnexinVnegCD45+ CD34+ CML-BC (fold-change relative to DMSO-treated ctrl)
P1
P4
Annexin V
CFSE
CD34+CFSE+ CML-BC

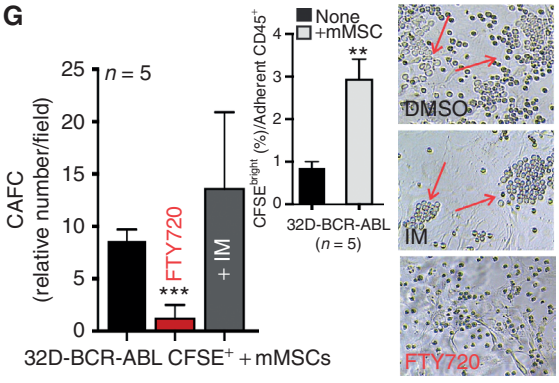
G
n = 5
CAFC (relative number/field)
FTY720
+ IM
32D-BCR-ABL CFSE+ + mMSCs
None
+mMSC
CFSEbright (%)/Adherent CD45+
32D-BCR-ABL (n = 5)
DMSO
IM
FTY720

DISCUSSION

Altered miRNA expression and PP2A tumor suppressor activity are tightly linked to leukemogenesis and impaired NK-cell–mediated anticancer immunity. The notion that PADs, but not TKIs, kill CML qLSCs (42) implies that BCR-ABL1 kinase-independent signals, likely arising from the endosteal hypoxic BMM (5), regulate CML LSC activity and survival through inhibition of PP2A. We previously reported that BCR-ABL1 expression, but not activity, is essential for recruitment of Jak2-driven hnRNPA1-mediated signals inducing SET-dependent PP2A inhibition that, in turn, allows CTNNB1 (β−catenin)-dependent regulation of CML (CP and BC) LSC proliferation and survival (9). We also demonstrated that inhibition of cytokine-induced SET upregulation or PAD treatment impair NK-cell cytotoxicity against Ph^+ cells through activation of PP2A (30). Here we showed that post-transcriptional signals, which are initiated by the tumor-naïve BMM and likely maintained by the tumor-reshaped BMM, control CML LSC entry/maintenance into quiescence and impair NK-cell immunity. This occurs through the induction of *MIR300*, a tumor suppressor miRNA with dose-dependent antiproliferative and PP2A-activating functions, which are uncoupled and differentially regulated by *TUG1* lncRNA decoy activity in CML LSCs. Importantly, a dose-dependent target selection mechanism (43) allows the sequential activation of *MIR300* antiproliferative and PP2A-activating functions through the inhibition of CDK6/CCND2 and SET, respectively, in CML qLSCs and progenitors and in NK cells.

MIR300 Role in CML LSCs and Progenitors

Expression studies revealed that *MIR300* levels are downregulated in CML (CP and BC) $CD34^+$ progenitors, but not in the CML-initiating (1) qLSC ($CD34^+CFSE^{max}$) fraction. Restoration of *MIR300* expression arrested proliferation, expanded the G_0–G_1 quiescent stem cell fraction, strongly impaired survival of dividing $CD34^+$ CML stem/progenitor cells, and was associated with downregulation of CCND2/CDK6, SET, and other PP2A-regulated CML growth- and survival-promoting factors (e.g., JAK2, CTNNB1, hnRNPA1 and MYC; ref. 1). Because CCND2/CDK6 inhibition characterizes quiescent long-term HSCs (LT-HSCs) and is sufficient to arrest $CD34^+$ leukemic progenitors in G_0–G_1 (21, 22), *MIR300*-induced loss of CCND2/CDK6, which occurs at low levels of *MIR300* expression, likely represents the mechanism by which *MIR300* antiproliferative activity contributes to CML stemness. Likewise, SET inhibition, which occurs when *MIR300* is highly expressed and is sufficient for triggering PP2A-mediated cell death of CML (CP and BC) qLSC and progenitors (8, 9), likely account for *MIR300*-induced apoptosis. In fact, we showed that loss of *MIR300* binding to SET impaired *MIR300*-induced PP2A-mediated Ph^+ cell apoptosis. This also suggests that inactivation and/or downregulation of JAK2, CTNNB1, Twist1, and MYC may result from *MIR300*-induced PP2A activation. Indeed, bioinformatics analysis that integrates several algorithms and also takes into account miRNA and mRNA targets' expression levels in normal and myeloid leukemia BM cells indicated that *MIR300*-induced inhibition of other PP2A-regulated survival factors (e.g., Twist1, CTNNB1, JAK2, and MYC) requires levels of *MIR300* significantly higher than those suppressing SET (Fig. 2B; Supplementary Fig. S3B). Thus, downregulation of these *MIR300* targets unlikely represent the primary mechanism of *MIR300*-induced apoptosis of CML qLSCs and progenitors. Strengthening the importance of CCND2/CDK6 and SET as key *MIR300* effectors is the notion that *MIR300*-induced CCND2/CDK6 and SET inhibition may not be limited to *MIR300*-induced posttranscriptional downregulation. In fact, *MIR300* may also impair SET, CCND2 and/or CDK6 transcription, mRNA nuclear export, translation and/or protein stability/activation upon inhibition of other PIP factors (e.g., hnRNPA1, JAK2, and SETBP1), and the associated XPO1 (Supplementary Fig. S3A, left; refs. 8, 20, 44–46).

The evidence that high levels of *MIR300* expression does not induce apoptosis of CML qLSCs, which exhibit inactivation of PP2A and activation of JAK2, SET, and CTNNB1 (1, 9), raises the questions of whether *MIR300* is required for LSC quiescence and survival; how *MIR300* is regulated in qLSCs and leukemic progenitors; and how qLSCs elude *MIR300*-induced apoptosis.

The requirement of *MIR300* for induction and maintenance of CML LSC quiescence is clearly demonstrated (Figs. 2D, 3B, and 4C; Supplementary Fig. S4D) by: (i) the ability of anti-*MIR300* molecules to antagonize MSC-induced inhibition of leukemic cell proliferation, (ii) impaired LTC-IC–driven colony formation in the absence of qLSC apoptosis in $CD34^+$ cells exposed to *CpG-miR-300* concentrations inhibiting CCND2/CDK6 but not SET expression, and by the (iii) inability of MSCs to induce SET downregulation in CML cells. Importantly, the evidence that *MIR300*-dependent SET inhibition is induced by hypoxia, but not MSCs, in $CD34^+$ CML stem/progenitor cells (Fig. 4A; Supplementary Fig. S4D) and that SET, JAK2, and CTNNB1 are active in CML qLSCs (1, 46), suggests that LSC entrance into quiescence is initiated by MSCs prior to LSC niching into the BM endosteal area with the lowest O_2 tension in which the *MIR300* PP2A-activating proapoptotic function is likely inhibited by the hypoxia-induced *TUG1* sponging activity. Moreover, the evidence that anti-*MIR300*–expressing MSCs fail to suppress leukemic $CD34^+$ cell proliferation, and that exposure of $CD34^+$ CML stem/progenitor cells to MSC CM and/or exosomes increases *MIR300* expression and double the number of $CD34^+$ CML cells in the quiescent LSC compartment (Fig. 4), suggests that the MSC-induced transition into quiescence of $CD34^+$ CML LSCs/progenitors may depend on CDK6/CCND2 downregulation induced by MSC-derived exosomal *MIR300*. In this scenario, hypoxia-induced *MIR300* will sustain, but not promote, CML LSC quiescence. However, MSCs may contribute to the hypoxia-dependent regulation of *MIR300*-induced LSC quiescence and qLSC survival by increasing *TUG1* expression through the release of TGFβ1 (36). Mechanistically, we showed that hypoxia induces *MIR300* transcription in $CD34^+$ CML cells and MSCs through reduced LIP (inhibitory) and increased LAP1 (activatory) C/EBPβ, which binds/transactivates a hypoxia-sensitive regulatory element located 109 bp upstream the *MIR300* gene. Accordingly, it was found that C/EBPβ was found expressed in CML LSCs (26), induced by hypoxia, and to negatively regulate G_1–S transition and SET expression (47, 48).

Although other miRNAs regulating LSC survival or qLSC reentry into cycle have been associated with CML development (18, 49, 50), to our knowledge, *MIR300* is the only cell

context–independent (same activity in LSCs and progenitors) miRNA capable of both supporting CML leukemogenesis by inducing LSC quiescence and triggering CML qLSC and progenitor cell apoptosis.

MIR300 Role in NK Cells

MIR300 is also the only tumor-naïve–induced tumor suppressor miRNA that inhibits NK cell–mediated innate anticancer immunity while promoting LSC quiescence. NK cells preferentially kill cancer stem cells (4, 51), including BM-repopulating TKI-resistant BCR-ABL1$^+$ qLSCs (Fig. 5B), and NK-cell quantitative and functional impairment is a feature of patients with untreated and TKI-treated CML (6, 52). Impaired NK-cell immunity also associates with CML qLSC persistance in patients with TKI-treated CML in deep molecular remission (28, 31), whereas normal levels of activated NK cells characterize patients in sustained treatment-free remission (28) and account for increased disease-free survival after T-cell–depleted stem cell transplant (4), suggesting that NK-cell–based therapies may lead to qLSC eradication.

Despite RNA sequencing (RNAseq) of MSC exosomal RNA suggesting that other 14 MSC-derived miRNAs may contribute to impaired NK-cell activity (Supplementary Fig. S5C), we showed that *MIR300* levels are increased in circulating NK cells from patients with CML at diagnosis and that BMM-induced inhibition of NK cell proliferation and antitumor activity require *MIR300* induction. In fact, BMM-induced NK cell inhibition was recapitulated by *MIR300* mimics and abrogated by *MIR300* RNAi. Furthermore, our data suggests that impaired NK-cell proliferation and cytotoxicity may depend on C/EBPβ-*MIR300* signals leading to CCND2/CDK6 and SET downregulation. Because the tumor-naïve BMM-induced loss of CCND2 and SET expression (PP2A inhibition) account for suppression of NK cell proliferation (29) and antitumor cytotoxicity (30), the NK cell quantitative and qualitative defects observed in CML may arise from *MIR300*-mediated signals initiated by the naïve BMM (53), sustained and/or exacerbated by the leukemia-reshaped BMM (54) and overriding cytokine-driven NK cell activation (55). Interestingly, treatment with MSC exosomes also reduced pre-miR-155 levels (BIC) in IL12/IL18-stimulated and resting NK-92 cells (Supplementary Fig. S5D). Because, miR-155 not only inhibits SHIP1 and PP2A to allow MAPK- and AKT-dependent NK cell proliferation and cytotoxic activity (16, 55), but also suppresses C/EBPβ expression (ref. 56; Supplementary Fig. S5D), MSC-induced BIC downregulation likely contributes to *MIR300*-dependent NK cell inhibition by antagonizing miR155-induced C/EBPβ downregulation. Furthermore, consistent with the notion that *TUG1* acts as a *MIR300* decoy and in contrast with the mechanism regulating *MIR300* activities in leukemic cells, BMM-induced NK cell inhibition occurs in a *MIR300*-dependent, but not *TUG1*-independent manner; in fact, hypoxia did not increase, but decreased *TUG1* expression in NK cells, and *TUG1*-shRNAs did not alter NK cell number (Supplementary Fig. S5E and S5F).

Biologic and Therapeutic Relevance of the *MIR300-TUG1* Interplay in CML Cells

TUG1 is an oncogenic lncRNA upregulated in different types of cancer in which it has strong diagnostic, prognostic and therapeutic relevance (34). In CML-BC qLSCs, *TUG1* is induced by hypoxia and uncouples *MIR300* functions and dose-dependently suppresses only *MIR300* PP2A-mediated proapoptotic activity (Fig. 6). This unprecedented lncRNA function allows *TUG1* to maintain unbound *MIR300* at levels sufficient for inducing CML LSC growth arrest but not for triggering PP2A-mediated apoptosis, which does not depend on loss of *TUG1* survival signals, but on the effect of freed *MIR300* on SET mRNA. Accordingly, *TUG1* loss in solid tumors was associated with G_0–G_1 arrest and apoptosis, whereas its overexpression with induction of proliferation and upregulation of mitogenic and survival factors (e.g., CCND1/2, CTNNB1, and Twist1) also described as *MIR300* targets (34). In addition, we showed that *TUG1* activity is *MIR300*-restricted in CD34$^+$ CML qLSCs, but not in leukemic progenitors in which TUG1-shRNAs induced apoptosis of anti-*MIR300*–treated CD34$^+$ CML cells. Because *TUG1* interacts with several tumor suppressor miRNAs (34, 57), this suggests that *TUG1* may function in CML LSCs and progenitors as a hub for specific subsets of functionally related tumor suppressor miRNAs. Indeed, 56 experimentally validated *TUG1*-interacting miRNAs that possess growth-suppressive and/or proapoptotic functions are differentially expressed in CD34$^+$CD38$^-$ LSC-enriched and CD34$^+$CD38$^+$–committed progenitor CML (CP and BC) cells (Supplementary Fig. S7A). Notably, 96.4% and 44.3% of these miRNAs are predicted to shut down BCR-ABL1–dependent signals in CML blasts and, like *MIR300*, to act as inhibitors of cell-cycle progression and PP2A activators (Supplementary Fig. S7A and S7B). Thus, it is conceivable that balanced *TUG1-MIR300* levels are essential for CML qLSC induction/maintenance, whereas insufficient *TUG1* expression will lead to CML qLSC and progenitor cell apoptosis by freeing *MIR300* and other miRNAs with similar tumor suppressor activities. Conversely, high *TUG1* sponge activity will likely promote CML cell proliferation, survival, and qLSC cell-cycle reentry, although an aberrant *TUG1* increase that also inhibits *MIR300* antiproliferative activity may induce LSC exhaustion by impairing entry into quiescence and forcing reentry into cycle.

Mechanistically, we showed that increased *TUG1* expression in qLSCs depends on hypoxia-induced TGFβ1 secretion by CD34$^+$ CML stem/progenitor cells. In fact, exposure to a TGFβ1 blocking antibody markedly impaired *TUG1* expression in CML progenitors and in hypoxia-cultured CML qLSCs. However, hypoxia-induced TGFBR1/2 upregulation in CML LSCs (36) may also contribute to increased *TUG1* expression and regulation of *MIR300* functions. Hypoxia-induced *TUG1* expression in CML qLSCs may also depend on Notch activity (58); however, blocking TGFβ1 signaling in CD34$^+$ CML progenitors and hypoxia-exposed qLSCs also strongly suppressed expression of FoxM1, a *TUG1* transcriptional inducer and regulator of CML LSC quiescence and cycling activity (37, 39, 50). Thus, hypoxia–TGFβ–FoxM1, but not Notch-induced signals, increases *TUG1* expression in CML LSCs to selectively inhibit *MIR300* PP2A-mediated proapoptotic function while allowing *MIR300*-dependent entry into quiescence. However, Notch signaling may contribute to the *MIR300-TUG1*–dependent regulation of LSC quiescence and survival through the RBPJ-mediated inhibition of miR-155 that may induce *TUG1* and *MIR300* expression by

preventing FoxM1 and C/EBPβ downregulation, respectively (Supplementary Fig. S6C).

In conclusion, tumor-naïve BMM-induced *MIR300* tumor suppressor antiproliferative and PP2A-activating functions support CML development through induction of LSC quiescence and inhibition of NK cell–mediated qLSC killing, respectively. This may represent the initial step leading to formation and expansion of the TKI-resistant CML qLSC pool. Once established, the CML clone will reshape the BMM to further support disease development and progression. *TUG1–MIR300* interaction plays a central role in this process because altering its ratio leads to the nearly complete and selective PP2A-dependent eradication of chronic and blastic CML qLSCs *in vitro* and in PDXs. This, together with the ability of SET-sequestering PADs to bypass the MSC-induced protective effect on CML qLSC survival, not only highlights the therapeutic importance of pharmacologically modulating PP2A activity in anti-LSC and NK cell–based therapeutic approaches for CML eradication, but also indicates that the activity of a tumor suppressor (i.e., *MIR300*) can be exploited by LSCs to preserve their ability to induce and maintain leukemia.

METHODS

Cell Culture and Treatments

Cell Lines Ph$^+$ CML-BC K562 and LAMA-84, human BM MSC–derived HS-5 (59), mouse BM–derived 32D-BCR/ABL, and the clinically relevant human NK-92 (60) cells were cultured in RPMI1640 medium. NK-92 cultures were supplemented with 150 IU/mL rhIL2 (Hoffmann-La Roche, Inc.). The amphotropic-packaging 293T and Phoenix cells were cultured in DMEM. All tissue culture media were supplemented with 10% to 20% heat-inactivated FBS (Gemini; Invitrogen), 2 mmol/L L-glutamine, and 100 U/mL penicillin/streptomycin (Invitrogen). Cell lines were obtained from ATCC, authenticated by FACS, qRT-PCR, or immunoblotting phenotypical analyses and used at low passages and tested for *Mycoplasma* contamination using a MycoAlert Mycoplasma Detection Kit (Lonza, Inc.).

Primary Cells Human hematopoietic stem and progenitor cell factions from healthy and leukemic individuals were isolated from BM, PB, or UCB. Prior to their use, cells were kept (18 hours) in StemSpan CC100 cytokine-supplemented SFMII serum-free medium (Stemcell Technologies). Human BM MSCs (hMSCs) from healthy individuals were isolated from BM cells by Ficoll-Hypaque density-gradient centrifugation followed by culture in complete human MesenCult Proliferation Kit medium and used for CM and exosome purification (Supplementary Methods). Human CD56$^+$CD3$^-$ NK cells (purity >95%) from healthy (UCB or PB), CML (CP, BC and AP) individuals were FACS and/or magnetic (Miltenyi Biotec, Inc.) cell sorted, or RosetteSep Ab-purified (Stemcell Technologies) as described previously (30).

Frozen CML leukemia specimens were from the Leukemia Tissue Banks located at The University of Maryland (UMB, Baltimore, MD), The Ohio State University (Columbus, OH), Maisonneuve-Rosemont Hospital Research Centre, Montreal (Quebec, Canada), Hammersmith Hospital, Imperial College (London, United Kingdom), "Policlinico-Vittorio Emanuele" (Catania, Italy), University of Utah (Salt Lake City, UT), Hematology Institute Charles University (Prague, Czech Republic), and Aarhus University Hospital (Aarhus, Denmark); fresh UCB, NBM, and PB (CML and healthy individuals) samples were purchased (Lonza, Inc.) or obtained from UMB Hospital (Baltimore, MD) and Maisonneuve-Rosemont Hospital Research Centre, Montreal. Patient samples were not collected for this study, which was carried out with a waiver of informed consent and approval from the University of Maryland Institutional Review Board (IRB). UCB units were collected at the University of Maryland Medical Center with IRB-approved protocol and written informed consent.

mMSCs were isolated as described previously (61). Briefly, BM was flushed from femurs and tibias of FVB/N mice. Bones were fragmented to small chips (1–2 mm) and digested with 1 mg/mL collagenase for 2 hours at 37°C. Digested bones were grown in mouse MesenCult MSC Basal Medium supplemented with Mesenpure and MSC Stimulatory Supplement (Stemcell Technologies). Purity (Lin$^-$CD45$^-$CD31$^-$CD51$^+$Sca1$^+$>90%) of isolated cells was confirmed by flow cytometry using anti-Lin Pacific Blue, CD45 Pe-Cy7, CD31 FITC (BioLegend), CD51 PE, and Sca1 APC (eBioscience) antibodies. Cells were kept for a maximum of five passages. mMSC CM was obtained by culturing 50% to 70% confluent mMSCs in IMDM supplemented with 10% FBS and 2 mmol/L L-glutamine for 48 hours.

Cells were treated for the indicated time and schedule with 1–2 μmol/L imatinib mesylate (IM; Novartis), 5 μmol/L 5-Aza-2′-deoxycytidine (5-Aza; Sigma), 250–500 nmol/L *CpG-scramble, -miR-300*, *-anti-miR-300*, and *-TUG1-shRNA* oligonucleotides (ODN; Beckman Research Institute, City of Hope, Duarte, CA), 1.25 μg/mL anti-TGFβ neutralizing antibody (1D11; R&D Systems), 10 ng/mL rhIL12 and 100 ng/mL rhIL18 (R&D Systems), and 2 μmol/L FTY720 (Fingolimod, Sigma). Where indicated, cells were cultured for the indicated times in hypoxic conditions (1% O_2), HS-5 and hMSC CM (100% vol/vol), or in medium supplemented with MSC-derived exosomes (50–100 μg/mL). During treatments, viable cells were enumerated by the trypan blue exclusion test.

Flow Cytometry and Cell Sorting

CD34$^+$, CD34$^+$CD38$^-$, CD34$^+$CD38$^+$ fractions were magnetic (CD34 MicroBead Kit; Miltenyi Biotec) and/or FACS (αCD34 APC/PE and αCD38 PE/Cy7 Abs, BD Biosciences) purified (purity: >90%–100%). Primary human NK cells were sorted using Alexa Fluor 488 αhCD56, PE-Cy5 αhCD19c and PE-Cy7 αhCD3 Abs (BD Biosciences) and their purity assessed by PE αCD56 (Beckman Coulter, Life Sciences) and APC-eFluor780 αCD3 (eBioscience) antibody staining. hMSC purity (>99%) was assessed by flow cytometry using anti-CD34 and CD45 FITC, CD73 PE-Cy7, CD105 Alexa 647, CD44 Percp-Cy5.5, and CD90 PE antibodies (BD Biosciences). Apoptosis was quantified by FACS upon staining cells with PE Annexin-V and 7-ADD (BD Biosciences). Cells were sorted using the FACS Aria II (BD Biosciences). Data acquisition and analyses were performed at the UMBCCC Flow Cytometry Facility. Data from LSRII or CANTO II flow cytometers (BD Biosciences) were analyzed by using either the FlowJo v8.8.7 or Diva v6.1.2 software.

LTC-IC and CFC/Replating Assays

CD34$^+$ CML (CP and BC) and UCB cells were lentivirally transduced/GFP-sorted and/or treated (500 nmol/L, 3 days) with *CpG-ODN* to ectopically express either *MIR300* or anti-*MIR300* RNAs prior to use in LTC-IC and CFC assays (46). Vector-transduced and CpG-scramble–treated cells served as controls.

LTC-ICs A total of 2×10^5 CML and 2×10^3 UCB CD34$^+$ cells were cultured with a 1:1 mixture of irradiated (80 Gy) IL3/G-CSF–producing M2-10B4 and IL3/KL–producing SI/SI murine fibroblasts in MyeloCult H5100 (Stemcell Technologies) supplemented with hydrocortisone. Medium was replaced after 7 days, followed by weekly half-medium changes, and fresh 500 nmol/L *CpG-ODN* where required. After 6 weeks, adherent and floating cells were harvested, and 5×10^3 CML and 2×10^3 for UCB cells were plated into cytokine (KL, G-CSF, GM-CSF, IL3, and IL6) supplemented MethoCult H4435. LTC-IC–derived colonies were scored after 14 days.

CFCs and CFC/replating Assays CD34$^+$ and CD34$^+$ CD38$^-$ CML (5×10^3) and/or UCB (2×10^3) cells were seeded in MethoCult H4435 supplemented with Epo, KL, G-CSF, GM-CSF, IL3, and IL6. Fourteen-day colonies were mixed and the same number of cells replated twice (first and second replating) and scored 2 weeks later.

CFSE (or eFluor670)-Mediated Tracking of Cell Division

CFSE (CellTrace CFSE Proliferation Kit, Invitrogen) or eFluor670 (Cell Proliferation Dye eFluor670; eBioscience)-stained cells were FACS sorted to isolate the highest fluorescent peak, treated as indicated, harvested after 4 to 5 days, and counterstained with Near-IR Fluorescent Dye (Live/Dead Cell Stain Kit, Invitrogen) to determine the number of viable dividing (CFSE/NearIR$^-$) and quiescent cells (CFSE^{max}/NearIR$^-$). Where indicated, cells were stained with anti-CD34 APC and sorted into dividing and quiescent subpopulations. Quiescent stem (CFSE^{max}CD34$^+$) and dividing progenitor cells in each peak were reported as a fraction of the initial number of CD34$^+$ cells (46). For NK cells, 4- and 7-day–cultured CFSE-labeled NK-92 and primary NK cells, respectively, were αCD56 APC Ab- and Aqua Fluorescent Dye (Live/Dead Cell Stain Kit, Invitrogen) stained. NK cells were used in cytotoxicity assays and proliferation was quantitated as fold changes of CFSE mean fluorescence intensity in living CD56$^+$ NK cells.

Plasmids

pCDH-miR-300 (hsa-*miR-300*) pCDH-*MIR300* was generated by subcloning a 490 bp *Nhe*I-*Bam*HI PCR fragment encompassing the mature hsa-*MIR300* into the pCDH-CMV-MCS-EF1-copGFP-puro (SBI) vector. Sequence was confirmed by sequencing.

pSIH-H1-Zip-MIR300 (pZip-MIR300) To knockdown *MIR300*, a 5′-*Eco*RI and 3′-*Bam*HI-flanked *MIR300* antisense dsODN was directionally cloned into the pSIH1-H1-copGFP vector (SBI).

pSIH-H1-copGFP-shTUG1 (TUG1 shRNA) A shRNA cassette containing the targeted nt 4571 to 4589 of hTUG1 RNA (58) was subcloned into pSIH-H1-copGFP vector (SBI). A nonfunctional scrambled *TUG1* shRNA was used as a control.

pLenti-TUG1 The h*TUG1* into the pLenti-GIII-CMV-GFP-2A-Puro–based vector was from Applied Biological Materials, Inc.

pGFP/Luc-based MIR300 Promoter Constructs p513-GFP/Luc, p245-GFP/Luc, and p109-GFP/Luc were generated by cloning the -522 bp, -245 bp, and -109 bp regions upstream the hsa-*MIR300* gene locus (Sequence ID: NC_000014.9) into pGreenFire1 (pGFP/Luc, pGF1; SBI) reporter vector. The regions upstream the hsa-*MIR300* gene were PCR amplified from K562 DNA and cloned into the pGF1 *Eco*RI-blunted site.

p109-C/EBPBmut-GFP/Luc An *Eco*RI-containing double-stranded synthetic oligonucleotide spanning the −109 bp *MIR300* regulatory (region and containing the T/G and C/G mutated C/EBPβ consensus binding sites located at positions -64 and -46, respectively, was subcloned into *Eco*RI-digested pGF1 vector. pCDH-Flag-SET, fluorescent ubiquitination–based cell-cycle indicator reporter pCDH-FUCCI2BL, MigR1-ΔuORF-C/EBPβ-ER^{TAM}, and MigR1-ΔuORF-C/EBPα-HA constructs were described previously (25, 62–64).

pCDH-Flag-SET 3′UTRwt-GFP and pCDH-Flag-SET Δ3′UTR-GFP Wild-type (627 bp) or 3′-deleted (513 bp) SET 3′UTRs were PCR amplified from K562 cDNA using a common EcoRI-linked 5′-primer and specific *Bam*HI-linked 3′-primers for the wild-type and deleted *SET* mRNA 3′UTR. The PCR products were cloned into the pCDH-Flag-SET plasmid and sequenced.

MSC CM and Exosome Purification

HS-5- and hMSC-derived CM was obtained by culturing cells in complete RPMI (24 hours) and StemSpan SFMII (48 hours) medium, respectively. Alix$^+$CD63$^+$ exosomes were purified by differential centrifugation (3,000 × *g*, 15 minutes; 10,000 × *g*, 10 minutes; and 100,000 × *g*, 70 minutes) from HS-5 CM cultured in exosome-free FBS-supplemented medium (65, 66). When required, exosomes were precipitated (Exo-Quick; SBI) prior to isolation by ultracentrifugation.

Lentiviral and Retroviral Transduction

Lentiviral or retroviral particles were produced by transient calcium phosphate transfection (ProFection Mammalian Transfection System, Promega) of 293T and Phoenix cells, respectively (8, 9, 67). Briefly, viral supernatant was collected 24 and 48 hours after transfection and directly used or concentrated by PEG precipitation. Viral titer was determined by flow cytometry by calculating number of GFP$^+$ 293T cells exposed (48 hours) to different viral dilutions. One to three spinoculation rounds were used for cell line infection, whereas a single spinoculation with diluted viral supernatants (MOI = 6) was used for primary cells. Viral supernatants were supplemented with polybrene (4 μg/mL). FACS sorting or puromycin selection was initiated 48 hours after transduction.

Cell-cycle Analysis

Cell-cycle analysis was performed by 4′,6′-diamidine-2-phenylindole (DAPI)/Ki-67 staining of *CpG-scramble*- or *CpG-miR-300*-treated (500 nmol/L; 72 hours) primary CD34$^+$ CML (CP and BC) and UBC cells as described previously (64). Briefly, cells were fixed, permeabilized (Cytofix/Cytoperm kit, BD Biosciences), and Ki-67 PE (BioLegend) and DAPI (Sigma) stained. Alternatively, cell-cycle analysis was performed on pCDH-Fucci2BL–infected cells and subjected to flow cytometric analysis. LAMA-84-FUCCI2BL$^+$ CML-BC cells were exposed to 500 nmol/L *CpG-scramble* and *CpG-miR-300* oligonucleotides after being G_1–S synchronized (4–6 μmol/L aphidicolin, 6 hours). *CpG-oligo*–treated (48 hours) FUCCI2BL$^+$ cells were subjected to live-cell imaging for 48 hours and analyzed as described previously (64). Briefly, *CpG-scramble*- or *CpG-miR-300*–treated cells in G_0–G_1 were mVenus$^-$ PE-Texas-Red$^+$, G_1–S cells were mVenus$^+$ PE-Texas-Red$^+$, and S–G_2–M cells were mVenus$^+$ PE-Texas-Red$^-$.

Live-Cell Imaging and Confocal Microscopy

Wide-field fluorescence imaging of *CpG-ODN*–treated pCDH-FUCCI2BL–transduced LAMA-84 cells was executed with an Olympus Vivaview digital camera, maintained at humidified atmosphere 37°C with 5% CO_2, mounted into a microscope-equipped incubator with green and red fluorescence filters. Emission spectral ranges were green-narrow (490–540 nm) and red-narrow (570–620 nm). Imaging was carried out for 24 or 48 hours. Confocal fluorescence images were acquired using a LEISS LSM510–inverted confocal microscope equipped with 40×/1.2-NA water immersion objective with 0.55-μm pixel size. Cell-cycle phases were determined by plotting average red and green fluorescent intensity over time using Prism 6.0 d software. The Vivaview raw images were reconstructed using ImageJ v5.2.5 and Adobe CS6 software.

Real-time RT-PCR

Total RNA was extracted using miRNeasy Micro Kit (Qiagen Inc.) or TRIzol (Invitrogen) and reverse transcribed using a standard cDNA synthesis or the TaqMan MicroRNA Reverse Transcription Kit

with mouse and/or human-specific sets of primers/probe for *BCR-ABL1, CEBPB, FOXM1, TUG1, IFNγ, pri-MIR300, MIR300, pre-miR-155 (BIC), 18S, RNU44, RNU6B*, and *snoRNA202* (Applied Biosystems). PCR reactions were performed using a StepOnePlus Real Time PCR System (Applied Biosystems). Data were analyzed according to the comparative C_t method using *RNU44, RNU6B, 18S*, and *snoRNA202* transcripts as an internal control. Results are expressed as fold change of mean ± SEM.

Immunoblot Analysis

Lysate from cell lines and primary cells were subjected to SDS-PAGE and Western blotting as described previously (46). The antibodies used were anti-actin, anti-Myc, anti-C/EBPβ, anti-Alix, anti-Twist, and anti-CD63 (Santa Cruz Biotechnology); anti-GRB2 (Transduction Laboratories); anti-JAK2, anti-β-catenin, anti-FoxM1, anti-CDK6, anti–pJAK2$^{Y1007/1008}$, and anti-CCND2 (Cell Signaling Technology); anti-SET (Globozymes); anti-ABL (Ab-3), anti-CCND1/2, anti-PY (4G10), and anti-PP2Ac^{Y307} (EMD); anti-hnRNPA1 (Abcam); and anti-Flag (M2; Sigma).

PP2A Phosphatase Assay

PP2A assays were performed using the malachite green–based PP2A Immunoprecipitation Phosphatase Assay Kit (Millipore) as described previously (46). Briefly, protein lysates (50 μg) in 100 μL of 20 mmol/L HEPES pH 7.0/100 mmol/L NaCl, 5 μg αPP2Ac Ab (Millipore), and 25 μL protein A–agarose was added to 400 μL of 50 mmol/L Tris pH 7.0, 100 mmol/L $CaCl_2$. Immunoprecipitates were carried out at 4°C for 2 hours and used in the phosphatase reaction according to the manufacturer's protocol.

Luciferase Assay

Transcriptional activity of the intergenic 513 bp region upstream the *MIR300* gene was investigated by luciferase assay using the pGreenFire-Lenti-Reporter system (pGF1; SBI) in cell lines and primary CD34$^+$ CML-BC cells. Briefly, cells were transduced with constructs containing wild-type full-length 513 (p513-GFP/Luc) and deleted 245 (p245-GFP/Luc) and 109 (p109-GFP/Luc) base pair–long region upstream the *MIR300* gene locus, or with the p109-GFP/Luc construct mutated in the two C/EBPβ-binding sites (p109-CEBPβmut-GFP/Luc). The empty vector (pGFP-Luc; pGF1) was used as a negative control. After 48 hours, cells were lysed and luciferase activity was determined by Pierce Firefly Luciferase Flash Assay Kit (Thermo Scientific).

Cytotoxicity Assays

A flow cytometry–based killing assay was performed using K562 cells as targets (68). Briefly, HS-5–derived CM (100% vol/vol) or exosomes (50–100 μg/mL) preconditioned (36 hours in 50–150 IU/mL IL2) NK-92 cells were coincubated (3.5 hours) with CFSE-labeled K562 cells at ratio 5:1. Killing was evaluated by assessing the percentage of Annexin-V$^+$ cells on CD56$^-$ and/or CFSE$^+$ target cells. When *CpG-ODNs* were used, NK-92 cells were preconditioned (36 hours) in medium lacking IL2. NK-92 cell-killing of qLSCs was performed using CFSE-labeled CD34$^+$ CML-BC cells cultured (4 days) in cytokine-supplemented StemSpan II Serum-Free Expansion Medium exposed (18 hours) to NK-92 cells. Spontaneous cytotoxicity toward qLSCs was determined by FACS-mediated evaluation of LSC numbers in Annexin V^{neg}CD34$^+$CFSE^{max} cells before and after exposure to NK-92 cells.

LSC Engraftment and Disease Development in NRG-SGM3 Mice

In vivo evaluation of changes in BM-repopulating LSCs was performed as described previously (40). A total of 10^6 BM CD34$^+$ CML ($n = 3$; >95% Ph$^+$; CP, AP, and BC) cells, treated (500 nmol/L, 48 hours) *ex vivo* with *CpG*-ODNs, were intravenously injected (4 mice/treatment group/patient sample) into sublethally irradiated (2.6 Gy) 6 to 8-week-old NOD.Cg-*Rag1*^{tm1Mom} *Il2rg*^{tm1Wjl} Tg(CMV-IL3, CSF2,KITLG)1Eav/J mice (NRG-SGM3; The Jackson Laboratory). Engraftment was assessed by anti-human CD45 (BD Biosciences) flow staining of intrafemur BM aspirates (46) at 2 weeks in *CpG-scramble* control groups and at 2, 4, and 12 weeks posttransplant in *CpG-MIR300*, *-TUG1shRNA*, and *MIR300+TUG1shRNA* CML-BC, AP, and CP, respectively. Animal studies were performed according to IRB- and Institutional Animal Care and Use Committee–approved protocols.

Oligonucleotides and Primers

The partially phosphothioated (*) 2′-O-Methyl ODNs were linked using 5 units of C3 carbon chain linker, $(CH2)_3$ (X). The ODNs were synthesized by the DNA/RNA Synthesis Laboratory, Beckman Research Institute of the City of Hope (Duarte, CA).

CpG-oligonucleotides and Probes

CpG-miR-300: 5′-g*g*tgcatcgatgcagg*g*g*g*gxxxxxuauacaagggcagacucucucu-3′

CpG-anti-miR-300: 5′-g*g*tgcatcgatgcagg*g*g*g*gxxxxxagagagagucugcccuuguaua-3′

CpG-Tug1-shRNA: 5′-g*g*tgcatcgatgcagg*g*g*g*gxxxxxuuacucugggcuucugcac-3′

CpG-scramble: 5′-g*g*tgcatcgatgcagg*g*g*g*gxxxxxguagaaccguacucgucacuua-3′

pCDH-CMV-MCS-EF1-copGFP-puro miRNA Constructs

MIR300(F): 5′-gctagctgtgactagttgtaccttag-3′; *MIR300 (R):* 5′-gatcctctcttccagaaagttcttg-3′

pSIH1-H1-copGFP Constructs

Zip-*MIR300* ODN: 5′-gatatgttcccgtctgagagagagaaggacagtcttctctctcagacgggaacatataaaaacttaa-3′

shTUG1(+): 5′-gatccgtgcagaagcccagagtaattcaagagattactctgggcttctgcacttttg-3′

shTUG1 (−): 5′-aattcaaaaagtgcagaagcccagagtaatctcttgaattactctgggctctgcacg-3′

pCDH-Flag-SET Constructs

SET3′UTRwt-GFP(F): 5′-gaattctagctttttcctcctttctctgtata-3′;
SET3′UTRwt-GFP(R): 5′-cggatccgtatacaagtcaaact-3′
SETΔ3′UTR-GFP(F): 5′-ggatccagagaaaagcatccaa-3′;
SETΔ3′UTR-GFP(R): 5′-cggatccgtatacaagtcaaact-3′

pGreenFire1

p522-pGF1(F): 5′-ccggaattccggcacgttttcagtatcaaatgct-3′
p245-pGF1(F): 5′-ccggaattccggtgaacctcttttactgtgactagttg-3′
p109-pGF1(F): 5′-ccggaattccggggtgtgctgctctcaccat-3′
Common(R): 5′-tgctctagagcaaatgatggcagtgacaggaa-3′

p109-C/EBPβ Mutant Construct

(+) strand ODN: 5′-aattc ggtgtgctgc tctcaccatg cagatcccat ctgtg tctct aaggc**tggc**t cct**ggag**ctg gtgggaactt agtcacagag gaaatggcct tcctgtcact gccatcattg-3′

(−) strand ODN: 5′-caatgatggc agtgacagga aggccatttc ctctgtgact aagttcccac cagctccagg agccagcctt agagacaca gatgggatct gcatggtgag agcagcacac cgaatt-3′

Bioinformatics Tools

Statistically significant ($P < 0.05$ with FDR correction) predicted and validated hsa-*miR-300* mRNA targets according to mRNA target

function and *MIR300* doses were identified using DIANAmicroT-CDS (diana.imis.athena-innovation.gr), ComiR (http://www.benoslab.pitt.edu/comir/), CSmiRTar (http://cosbi4.ee.ncku.edu.tw/CSmiRTar/), and mirDIP 4.1 (ophid.utoronto.ca/mirDIP/; refs. 69–71). KEGG and GO analyses were used to define the biological pathways and the functional roles of miRNA-300 and *TUG1* targets were performed using miR-Path v.3 (snf-515788.vm.okeanos.grnet.gr). *MIR300* and *TUG1* individual gene expression profiles were obtained from curated datasets in the Gene Expression Omnibus (GEO) repository (ncbi.nlm.nih.gov/geoprofiles/). TUG1 levels in normal and leukemic myelopoiesis were analyzed from BloodSpot database (servers.binf.ku.dk/bloodspot/) of healthy and malignant hematopoiesis. Integration of StarBase v2.0 (starbase.sysu.edu.cn/starbase2/index.php) database with the RNAseq MiRbase data from $CD34^+CD38^-$, $CD34^+CD38^+$ CML and NBM cells was used to identify *TUG1*–sponged miRNAs.

Statistical Analysis

P values were calculated by Student *t* test (GraphPad Prism v6.0). Results are shown as mean ± SEM. A *P* value less than 0.05 was considered significant (*, $P < 0.05$; **, $P < 0.01$; ***, $P < 0.001$; ****, $P < 0.0001$). Mixed models' approach, the split-plot design, was used to assess differences in percent cell across three treatment groups. The percent cell change was estimated using a model with two main effects for treatment and stage of a cell cycle, as well as their interaction. Tests of fixed effects revealed that interaction of treatment and stage of a cell cycle is highly significant ($P = 0.01$) and the two main effects, treatment and stage, should be interpreted with caution (*P* values are 1.0 and <0.0001, respectively). The differences in average percent cell were tested across groups and sliced at a particular stage of cell cycle.

Disclosure of Potential Conflicts of Interest

D. Perrotti has ownership interest in patents 8,633,161; 9,220,706 and 8,318,812. P. Neviani has ownership interest in patents 9,220,706; 8,633,161. C.J. Walker is a consultant at Karyopharm Therapeautics, Inc. F. Stagno has received speakers bureau honoraria from Novartis, Bristol-Myers Squibb, Pfizer, and Incyte. P. Vigneri reports receiving a commercial research grant from Novartis, has received speakers bureau honoraria from Incyte, is a consultant/advisory board member for Incyte. M.W. Deininger is a consultant/advisory board member at Blueprint, Fusion Pharma, Novartis, Sangamo, Takeda, Medscape, Incyte, Ascentage Pharma, Humana, TRM and reports receiving commercial research grants from Blueprint, Takeda, Novartis, Incyte, SPARC, Leukemia & Lymphoma Society, and Pfizer. D. Milojkovic has received speakers bureau honoraria from Novartis, Bristol-Myers Squibb, Incyte, and Pfizer. No potential conflicts of interest were disclosed by the other authors.

Authors' Contributions

G. Silvestri: Investigation and methodology. **R. Trotta:** Supervision, funding acquisition, investigation, methodology, writing–review, and editing. **L. Stramucci:** Investigation. **J.J. Ellis:** Investigation. **J.G. Harb:** Investigation. **P. Neviani:** Investigation. **S. Wang:** Investigation. **A. Eisfeld:** Resources. **C.J. Walker:** Resources. **B. Zhang:** Resources. **K. Srutova:** Validation and investigation. **C. Gambacorti-Passerini:** Resources. **G. Pineda:** Resources. **C.H.M. Jamieson:** Resources. **F. Stagno:** Resources. **P. Vigneri:** Resources. **G. Nteliopoulos:** Resources. **P.C. May:** Resources. **A.G. Reid:** Resources. **R. Garzon:** Resources. **D. Roy:** Resources. **M.M. Moutuou:** Investigation. **M. Guimond:** Resources and investigation. **P. Hokland:** Resources. **M.W. Deininger:** Resources. **G. Fitzgerald:** Resources. **C. Harman:** Resources. **F. Dazzi:** Resources. **D. Milojkovic:** Resources. **J.F. Apperley:** Resources. **G. Marcucci:** Resources. **J. Qi:** Resources. **K. Machova Polakova:** Resources and investigation. **Y. Zou:** Investigation. **X. Fan:** Resources and investigation. **M.R. Baer:** Resources. **B. Calabretta:** Resources, writing–review, and editing. **D. Perrotti:** Conceptualization, formal analysis, supervision, funding acquisition, writing–original draft, writing–review, and editing.

Acknowledgments

This work was supported by grants from the NIH-NCI CA163800 and DOD W81XWH1910166 (to D. Perrotti), ACS IRG16-123-13 Pilot Grant (to R. Trotta), Maryland Cigarette Restitution Funds (UMB Greenebaum Comprehensive Cancer Center), MSMT CZ LH15104 (to K. Machova Polakova) and CRS 16255 (to M. Guimond) for patient sample procurement and processing. S. Wang was supported by a grant from the China NSFC 81872924 and Scholarship Council (file no. 201807060002). We thank O. Goloubeva for statistical data analysis; K.F. Underwood, J.R.H. Mauban, T. Pomicter, V.H. Duong, A. Emadi, A.M. Eiring, and N.M. Glynn-Cunningham for patient sample procurement, technical assistance, reagents, and/or critical reading of the manuscript.

The costs of publication of this article were defrayed in part by the payment of page charges. This article must therefore be hereby marked *advertisement* in accordance with 18 U.S.C. Section 1734 solely to indicate this fact.

Received October 9, 2019; revised December 27, 2019; accepted February 11, 2020; published first March 4, 2020.

Abbreviations: 5-Aza-2′-deoxycytidine (5-Aza); blast crisis (BC); bone marrow (BM) microenvironment (BMM); carboxyfluorescein diacetate succinimidyl diester (CFSE); CCAAT enhancer binding protein (C/EBP); colony forming cells (CFC); chronic myelogenous leukemia (CML); chronic phase (CP); cobblestone area forming cell (CAFC); conditioned medium (CM); hematopoietic stem cell (HSC); imatinib (IM); leukemic stem cells (LSC); long term culture–initiating cells (LTC-IC); luciferase (luc); mesenchymal stromal cells (MSC); natural killer (NK); normal BM (NBM); peripheral blood (PB); PP2A activating drugs (PAD); PP2A inhibiting drugs (PID); PP2A inhibitory pathway (PIP); protein phosphatase 2A (PP2A); quiescent leukemic stem cells (qLSCs); taurine upregulated gene 1 (TUG1); tyrosine kinase inhibitors (TKI); umbilical cord blood (UCB).

REFERENCES

1. Holyoake TL, Vetrie D. The chronic myeloid leukemia stem cell: stemming the tide of persistence. Blood 2017;129:1595–606.
2. Radich JP, Deininger M, Abboud CN, Altman JK, Berman E, Bhatia R, et al. Chronic myeloid leukemia, version 1.2019, NCCN clinical practice guidelines in oncology. J Natl Compr Canc Netw 2018;16:1108–35.
3. Corbin AS, Agarwal A, Loriaux M, Cortes J, Deininger MW, Druker BJ. Human chronic myeloid leukemia stem cells are insensitive to imatinib despite inhibition of BCR-ABL activity. J Clin Invest 2011;121:396–409.
4. Yong AS, Keyvanfar K, Hensel N, Eniafe R, Savani BN, Berg M, et al. Primitive quiescent CD34+ cells in chronic myeloid leukemia are targeted by in vitro expanded natural killer cells, which are functionally enhanced by bortezomib. Blood 2009;113:875–82.
5. Shah M, Bhatia R. Preservation of quiescent chronic myelogenous leukemia stem cells by the bone marrow microenvironment. Adv Exp Med Biol 2018;1100:97–110.
6. Carlsten M, Jaras M. Natural killer cells in myeloid malignancies: immune surveillance, NK cell dysfunction, and pharmacological opportunities to bolster the endogenous NK cells. Front Immunol 2019;10:2357.

7. Ruvolo PP. The broken "Off" switch in cancer signaling: PP2A as a regulator of tumorigenesis, drug resistance, and immune surveillance. BBA Clin 2016;6:87–99.
8. Neviani P, Santhanam R, Trotta R, Notari M, Blaser BW, Liu S, et al. The tumor suppressor PP2A is functionally inactivated in blast crisis CML through the inhibitory activity of the BCR/ABL-regulated SET protein. Cancer Cell 2005;8:355–68.
9. Neviani P, Harb JG, Oaks JJ, Santhanam R, Walker CJ, Ellis JJ, et al. PP2A-activating drugs selectively eradicate TKI-resistant chronic myeloid leukemic stem cells. J Clin Invest 2013;123:4144–57.
10. Agarwal A, MacKenzie RJ, Pippa R, Eide CA, Oddo J, Tyner JW, et al. Antagonism of SET using OP449 enhances the efficacy of tyrosine kinase inhibitors and overcomes drug resistance in myeloid leukemia. Clin Cancer Res 2014;20:2092–103.
11. Perrotti D, Agarwal A, Lucas CM, Narla G, Neviani P, Odero MD, et al. Comment on "PP2A inhibition sensitizes cancer stem cells to ABL tyrosine kinase inhibitors in BCR-ABL human leukemia". Sci Transl Med 2019;11:eaau0416.
12. Lai D, Chen M, Su J, Liu X, Rothe K, Hu K, et al. PP2A inhibition sensitizes cancer stem cells to ABL tyrosine kinase inhibitors in BCR-ABL(+) human leukemia. Sci Transl Med 2018;10:eaan8735.
13. Krause DS, Scadden DT. A hostel for the hostile: the bone marrow niche in hematologic neoplasms. Haematologica 2015;100:1376–87.
14. Cheloni G, Poteti M, Bono S, Masala E, Mazure NM, Rovida E, et al. The leukemic stem cell niche: adaptation to "Hypoxia" versus oncogene addiction. Stem Cells Int 2017;2017:4979474.
15. Saultz JN, Freud AG, Mundy-Bosse BL. MicroRNA regulation of natural killer cell development and function in leukemia. Mol Immunol 2019;115:12–20.
16. Ruvolo PP. The interplay between PP2A and microRNAs in leukemia. Front Oncol 2015;5:43.
17. Roden C, Lu J. MicroRNAs in control of stem cells in normal and malignant hematopoiesis. Curr Stem Cell Rep 2016;2:183–96.
18. Zhang B, Nguyen LXT, Li L, Zhao D, Kumar B, Wu H, et al. Bone marrow niche trafficking of miR-126 controls the self-renewal of leukemia stem cells in chronic myelogenous leukemia. Nat Med 2018;24:450–62.
19. Zhang JQ, Chen S, Gu JN, Zhu Y, Zhan Q, Cheng DF, et al. MicroRNA-300 promotes apoptosis and inhibits proliferation, migration, invasion and epithelial-mesenchymal transition via the Wnt/beta-catenin signaling pathway by targeting CUL4B in pancreatic cancer cells. J Cell Biochem 2018;119:1027–40.
20. Walker CJ, Oaks JJ, Santhanam R, Neviani P, Harb JG, Ferenchak G, et al. Preclinical and clinical efficacy of XPO1/CRM1 inhibition by the karyopherin inhibitor KPT-330 in Ph+ leukemias. Blood 2013;122:3034–44.
21. Jena N, Deng M, Sicinska E, Sicinski P, Daley GQ. Critical role for cyclin D2 in BCR/ABL-induced proliferation of hematopoietic cells. Cancer Res 2002;62:535–41.
22. Laurenti E, Frelin C, Xie S, Ferrari R, Dunant CF, Zandi S, et al. CDK6 levels regulate quiescence exit in human hematopoietic stem cells. Cell Stem Cell 2015;16:302–13.
23. Moradi S, Sharifi-Zarchi A, Ahmadi A, Mollamohammadi S, Stubenvoll A, Gunther S, et al. Small RNA sequencing reveals Dlk1-Dio3 locus-embedded MicroRNAs as major drivers of ground-state pluripotency. Stem Cell Reports 2017;9:2081–96.
24. Desplat V, Faucher JL, Mahon FX, Dello Sbarba P, Praloran V, Ivanovic Z. Hypoxia modifies proliferation and differentiation of CD34(+) CML cells. Stem Cells 2002;20:347–54.
25. Guerzoni C, Bardini M, Mariani SA, Ferrari-Amorotti G, Neviani P, Panno ML, et al. Inducible activation of CEBPB, a gene negatively regulated by BCR/ABL, inhibits proliferation and promotes differentiation of BCR/ABL-expressing cells. Blood 2006;107:4080–9.
26. Hayashi Y, Hirai H, Kamio N, Yao H, Yoshioka S, Miura Y, et al. C/EBPbeta promotes BCR-ABL-mediated myeloid expansion and leukemic stem cell exhaustion. Leukemia 2013;27:619–28.
27. Pierson BA, Miller JS. CD56+bright and CD56+dim natural killer cells in patients with chronic myelogenous leukemia progressively decrease in number, respond less to stimuli that recruit clonogenic natural killer cells, and exhibit decreased proliferation on a per cell basis. Blood 1996;88:2279–87.
28. Ilander M, Olsson-Stromberg U, Schlums H, Guilhot J, Bruck O, Lahteenmaki H, et al. Increased proportion of mature NK cells is associated with successful imatinib discontinuation in chronic myeloid leukemia. Leukemia 2017;31:1108–16.
29. Siegel G, Schafer R, Dazzi F. The immunosuppressive properties of mesenchymal stem cells. Transplantation 2009;87(9 Suppl):S45–9.
30. Trotta R, Ciarlariello D, Dal Col J, Mao H, Chen L, Briercheck E, et al. The PP2A inhibitor SET regulates granzyme B expression in human natural killer cells. Blood 2011;117:2378–84.
31. Hughes A, Yong ASM. Immune effector recovery in chronic myeloid leukemia and treatment-free remission. Front Immunol 2017;8:469.
32. Holyoake T, Jiang X, Eaves C, Eaves A. Isolation of a highly quiescent subpopulation of primitive leukemic cells in chronic myeloid leukemia. Blood 1999;94:2056–64.
33. Ma F, Wang SH, Cai Q, Jin LY, Zhou D, Ding J, et al. Long non-coding RNA TUG1 promotes cell proliferation and metastasis by negatively regulating miR-300 in gallbladder carcinoma. Biomed Pharmacother 2017;88:863–9.
34. Ghaforui-Fard S, Vafaee R, Taheri M. Taurine-upregulated gene 1: a functional long noncoding RNA in tumorigenesis. J Cell Physiol 2019;234:17100–12.
35. Qin CF, Zhao FL. Long non-coding RNA TUG1 can promote proliferation and migration of pancreatic cancer via EMT pathway. Eur Rev Med Pharmacol Sci 2017;21:2377–84.
36. Blank U, Karlsson S. TGF-beta signaling in the control of hematopoietic stem cells. Blood 2015;125:3542–50.
37. Hou Y, Li W, Sheng Y, Li L, Huang Y, Zhang Z, et al. The transcription factor Foxm1 is essential for the quiescence and maintenance of hematopoietic stem cells. Nat Immunol 2015;16:810–8.
38. Li Y, Zhang T, Zhang Y, Zhao X, Wang W. Targeting the FOXM1-regulated long noncoding RNA TUG1 in osteosarcoma. Cancer Sci 2018;109:3093–104.
39. Mancini M, Castagnetti F, Soverini S, Leo E, De Benedittis C, Gugliotta G, et al. FOXM1 transcription factor: a new component of chronic myeloid leukemia stem cell proliferation advantage. J Cell Biochem 2017;118:3968–75.
40. Abraham SA, Hopcroft LE, Carrick E, Drotar ME, Dunn K, Williamson AJ, et al. Dual targeting of p53 and c-MYC selectively eliminates leukaemic stem cells. Nature 2016;534:341–6.
41. Copland M, Hamilton A, Elrick LJ, Baird JW, Allan EK, Jordanides N, et al. Dasatinib (BMS-354825) targets an earlier progenitor population than imatinib in primary CML but does not eliminate the quiescent fraction. Blood 2006;107:4532–9.
42. Ciccone M, Calin GA, Perrotti D. From the biology of PP2A to the PADs for therapy of hematologic malignancies. Front Oncol 2015;5:21.
43. Shu J, Xia Z, Li L, Liang ET, Slipek N, Shen D, et al. Dose-dependent differential mRNA target selection and regulation by let-7a-7f and miR-17-92 cluster microRNAs. RNA Biol 2012;9:1275–87.
44. Eiring AM, Neviani P, Santhanam R, Oaks JJ, Chang JS, Notari M, et al. Identification of novel posttranscriptional targets of the BCR/ABL oncoprotein by ribonomics: requirement of E2F3 for BCR/ABL leukemogenesis. Blood 2008;111:816–28.
45. Konishi H, Fujiya M, Ueno N, Moriichi K, Sasajima J, Ikuta K, et al. microRNA-26a and -584 inhibit the colorectal cancer progression through inhibition of the binding of hnRNP A1-CDK6 mRNA. Biochem Biophys Res Commun 2015;467:847–52.
46. Perrotti D, Neviani P. Protein phosphatase 2A: a target for anticancer therapy. Lancet Oncol 2013;14:e229–38.
47. Du C, Pan P, Jiang Y, Zhang Q, Bao J, Liu C. Microarray data analysis to identify crucial genes regulated by CEBPB in human SNB19 glioma cells. World J Surg Oncol 2016;14:258.
48. Luedde T, Duderstadt M, Streetz KL, Tacke F, Kubicka S, Manns MP, et al. C/EBP beta isoforms LIP and LAP modulate progression of the cell cycle in the regenerating mouse liver. Hepatology 2004;40:356–65.
49. Zipeto MA, Court AC, Sadarangani A, Delos Santos NP, Balaian L, Chun HJ, et al. ADAR1 activation drives leukemia stem cell self-renewal by impairing let-7 biogenesis. Cell Stem Cell 2016;19:177–91.

50. Pellicano F, Park L, Hopcroft LEM, Shah MM, Jackson L, Scott MT, et al. hsa-mir183/EGR1-mediated regulation of E2F1 is required for CML stem/progenitor cell survival. Blood 2018;131:1532–44.
51. Kijima M, Gardiol N, Held W. Natural killer cell mediated missing-self recognition can protect mice from primary chronic myeloid leukemia in vivo. PLoS One 2011;6:e27639.
52. Baginska J, Viry E, Paggetti J, Medves S, Berchem G, Moussay E, et al. The critical role of the tumor microenvironment in shaping natural killer cell-mediated anti-tumor immunity. Front Immunol 2013;4:490.
53. Hasmim M, Messai Y, Ziani L, Thiery J, Bouhris JH, Noman MZ, et al. Critical role of tumor microenvironment in shaping NK cell functions: implication of hypoxic stress. Front Immunol 2015;6:482.
54. Schepers K, Campbell TB, Passegue E. Normal and leukemic stem cell niches: insights and therapeutic opportunities. Cell Stem Cell 2015;16:254–67.
55. Trotta R, Chen L, Costinean S, Josyula S, Mundy-Bosse BL, Ciarlariello D, et al. Overexpression of miR-155 causes expansion, arrest in terminal differentiation and functional activation of mouse natural killer cells. Blood 2013;121:3126–34.
56. Costinean S, Sandhu SK, Pedersen IM, Tili E, Trotta R, Perrotti D, et al. Src homology 2 domain-containing inositol-5-phosphatase and CCAAT enhancer-binding protein beta are targeted by miR-155 in B cells of Emicro-MiR-155 transgenic mice. Blood 2009;114:1374–82.
57. Zhao L, Sun H, Kong H, Chen Z, Chen B, Zhou M. The Lncrna-TUG1/EZH2 axis promotes pancreatic cancer cell proliferation, migration and EMT phenotype formation through sponging Mir-382. Cell Physiol Biochem 2017;42:2145–58.
58. Katsushima K, Natsume A, Ohka F, Shinjo K, Hatanaka A, Ichimura N, et al. Targeting the Notch-regulated non-coding RNA TUG1 for glioma treatment. Nat Commun 2016;7:13616.
59. Traer E, MacKenzie R, Snead J, Agarwal A, Eiring AM, O'Hare T, et al. Blockade of JAK2-mediated extrinsic survival signals restores sensitivity of CML cells to ABL inhibitors. Leukemia 2012;26:1140–3.
60. Klingemann H, Boissel L, Toneguzzo F. Natural killer cells for immunotherapy - advantages of the NK-92 cell line over blood NK cells. Front Immunol 2016;7:91.
61. Schepers K, Pietras EM, Reynaud D, Flach J, Binnewies M, Garg T, et al. Myeloproliferative neoplasia remodels the endosteal bone marrow niche into a self-reinforcing leukemic niche. Cell Stem Cell 2013;13:285–99.
62. Oaks JJ, Santhanam R, Walker CJ, Roof S, Harb JG, Ferenchak G, et al. Antagonistic activities of the immunomodulator and PP2A-activating drug FTY720 (Fingolimod, Gilenya) in Jak2-driven hematologic malignancies. Blood 2013;122:1923–34.
63. Eiring AM, Harb JG, Neviani P, Garton C, Oaks JJ, Spizzo R, et al. miR-328 functions as an RNA decoy to modulate hnRNP E2 regulation of mRNA translation in leukemic blasts. Cell 2010;140:652–65.
64. Pineda G, Lennon KM, Delos Santos NP, Lambert-Fliszar F, Riso GL, Lazzari E, et al. Tracking of normal and malignant progenitor cell cycle transit in a defined niche. Sci Rep 2016;6:23885.
65. Roccaro AM, Sacco A, Maiso P, Azab AK, Tai YT, Reagan M, et al. BM mesenchymal stromal cell-derived exosomes facilitate multiple myeloma progression. J Clin Invest 2013;123:1542–55.
66. Thery C, Amigorena S, Raposo G, Clayton A. Isolation and characterization of exosomes from cell culture supernatants and biological fluids. Curr Protoc Cell Biol 2006;Chapter 3:Unit 3 22.
67. Neviani P, Santhanam R, Oaks JJ, Eiring AM, Notari M, Blaser BW, et al. FTY720, a new alternative for treating blast crisis chronic myelogenous leukemia and Philadelphia chromosome-positive acute lymphocytic leukemia. J Clin Invest 2007;117:2408–21.
68. Romee R, Rosario M, Berrien-Elliott MM, Wagner JA, Jewell BA, Schappe T, et al. Cytokine-induced memory-like natural killer cells exhibit enhanced responses against myeloid leukemia. Sci Transl Med 2016;8:357ra123.
69. Coronnello C, Benos PV. ComiR: combinatorial microRNA target prediction tool. Nucleic Acids Res 2013;41:W159–64.
70. Tokar T, Pastrello C, Rossos AEM, Abovsky M, Hauschild AC, Tsay M, et al. mirDIP 4.1-integrative database of human microRNA target predictions. Nucleic Acids Res 2018;46:D360–70.
71. Wu WS, Tu BW, Chen TT, Hou SW, Tseng JT. CSmiRTar: condition-specific microRNA targets database. PLoS One 2017;12:e0181231.